Am J Physiol Cell Physiol 307: C320–C337, 2014.
First published June 4, 2014; doi:10.1152/ajpcell.00068.2013.

Transepithelial glucose transport and Na^+/K^+ homeostasis in enterocytes: an integrative model

Kristian Thorsen,[1] Tormod Drengstig,[1] and Peter Ruoff[2]

[1]*Department of Electrical Engineering and Computer Science, University of Stavanger, Stavanger, Norway; and* [2]*Centre for Organelle Research, University of Stavanger, Stavanger, Norway*

Submitted 5 March 2013; accepted in final form 1 June 2014

Thorsen K, Drengstig T, Ruoff P. Transepithelial glucose transport and Na^+/K^+ homeostasis in enterocytes: an integrative model. *Am J Physiol Cell Physiol* 307: C320–C337, 2014. First published June 4, 2014; doi:10.1152/ajpcell.00068.2013.—The uptake of glucose and the nutrient coupled transcellular sodium traffic across epithelial cells in the small intestine has been an ongoing topic in physiological research for over half a century. Driving the uptake of nutrients like glucose, enterocytes must have regulatory mechanisms that respond to the considerable changes in the inflow of sodium during absorption. The Na-K-ATPase membrane protein plays a major role in this regulation. We propose the hypothesis that the amount of active Na-K-ATPase in enterocytes is directly regulated by the concentration of intracellular Na^+ and that this regulation together with a regulation of basolateral K permeability by intracellular ATP gives the enterocyte the ability to maintain ionic Na^+/K^+ homeostasis. To explore these regulatory mechanisms, we present a mathematical model of the sodium coupled uptake of glucose in epithelial enterocytes. Our model integrates knowledge about individual transporter proteins including apical SGLT1, basolateral Na-K-ATPase, and GLUT2, together with diffusion and membrane potentials. The intracellular concentrations of glucose, sodium, potassium, and chloride are modeled by nonlinear differential equations, and molecular flows are calculated based on experimental kinetic data from the literature, including substrate saturation, product inhibition, and modulation by membrane potential. Simulation results of the model without the addition of regulatory mechanisms fit well with published short-term observations, including cell depolarization and increased concentration of intracellular glucose and sodium during increased concentration of luminal glucose/sodium. Adding regulatory mechanisms for regulation of Na-K-ATPase and K permeability to the model show that our hypothesis predicts observed long-term ionic homeostasis.

enterocytes; epithelial transport; homeostasis; mathematical modeling; ionic regulation

THE UPTAKE AND TRANSPORT OF glucose by the epithelial enterocytes in the small intestine are essential steps in all higher animals. Much of the glucose uptake in the small intestine is coupled to transport of sodium, and the different transporter proteins involved in the sodium coupled glucose uptake are well known (23, 61, 67, 97). Although the electrochemical kinetics of the individual transporter proteins responsible for glucose and nutrient uptake are fairly elucidated (19, 54, 67, 82, 97), the combined function in which these transporters drive a net inflow of nutrients from the intestinal lumen to the serosal blood has not yet been modeled in detail.

We have developed a mathematical model of an enterocyte that incorporates the available kinetic data from studies on individual transporter proteins. The model includes apical SGLT1 (the glucose sodium cotransporter), coupled apical flow of Na^+ and Cl^-, basolateral Na-K-ATPase (the sodium potassium pump), basolateral GLUT2 (the facilitated glucose transporter), and diffusive flows of the three included ionic species: Na^+, K^+, and Cl^- (see Fig. 1). The model also incorporates the dynamically changing electrochemical potential between the intestinal lumen (mucosal), the inside of the enterocyte (cell), and the inner extracellular site (serosal). There is a membrane potential between the mucosal side and the cell inside ψ_{mc}, between the serosal side and the cell inside ψ_{sc}, and a potential from the mucosal side to the serosal side, over the epithelial cells ψ_{ms} (see Fig. 1).

While there are no detailed mathematical models of enterocytes, several models exist for other epithelial cells. A model for transport of Na^+, K^+, and Cl^- in Necturus gallbladder epithelium was developed by Baerentsen et al. in 1982 (2). At that time little was known on the existence and kinetics of different transporter proteins, so their model was based on diffusion and an expression for the flow through Na-K-ATPase. Noteworthy is also the work of Stephenson and Weinstein (78, 96), and later Weinstein alone (87–90, 91, 93, 95), which mainly focused on models of kidney epithelium. Weinstein's model of the rat proximal tubule is particularly remarkable; this model has been developed and refined continuously over decades. It started with a cell centric model based on a metabolically active Na-K-ATPase and passive membrane transport based on linear equations from nonlinear thermodynamics (87); linear glucose and sodium cotransport was added in Ref. 88. The model was extended to represent a segment of tubule epithelium (89) and then further extended with pathways for Cl^- transport (90) and ammonia (91). Our enterocyte model is not based on any of these models, i.e., it is not an old model with new parameters. It is instead a fresh start where we have tried to use the available knowledge from studies on individual transporter proteins to employ flow expressions that are based on kinetics rather than linear relations.

In doing its job, the epithelial enterocyte is able to deal with a rapidly changing and often large inflow of Na^+ (72). This requires that the enterocyte possesses intracellular regulatory mechanisms that adjust the compensatory ionic flows to maintain homeostasis. It is known that the inflow of sodium through uptake of glucose and amino acids leads to an increased Na-K-ATPase pump activity (72, 73) and a corresponding increase in basolateral K permeability (7, 22, 28). We will test the hypothesis that these responses, which enable homeostasis of intracellular Na^+ and K^+, are achieved by a direct regulation of Na-K-ATPase production by intracellular Na^+ together with a regulation of the basolateral permeability for K^+ based on the Na-K-ATPase pump rate. The enterocyte also faces the same challenges as other transporting epithelia in maintaining

Address for reprint requests and other correspondence: K. Thorsen. Univ. of Stavanger, 4036 Stavanger, Norway (e-mail: kristian.thorsen@uis.no).

other properties such as cell volume and pH value, but we are in this work primarily interested in ionic homeostasis. It should be mentioned that some of the other models of epithelial cells have also been used to investigate homeostatic mechanisms (93, 95), although not for enterocytes.

We consider our enterocyte model as a valuable tool for assessment of hypothetical regulatory mechanisms. The model provides a quantitative framework where plausible mechanisms for regulation and adaptation to changes, like altered nutrient load or cell aging, can be tested. Our model is, to our knowledge, the first integrative approach to model both short and long-term phenomena in enterocytes.

Physiological Work Mode

In the small intestine, carbohydrates are hydrolyzed to disaccharides by pancreatic enzymes and further hydrolyzed into glucose, galactose, and fructose by enzymes at the brush border membrane of the epithelial enterocytes.

Glucose and galactose transport from the intestine consists of both a saturable component and a nonsaturable component (32). It is generally agreed upon that the saturable component stems from active transport via SGLT1, whereas the nonsaturable component is argued to stem from either solvent drag and paracellular flow a theory advocated by Pappenheimer and Reiss (63) or from trafficking of GLUT2 to the apical membrane at higher luminal glucose concentrations (36). In this work we only consider the saturable component, which contributes most to the transport at low glucose concentrations.

Figure 1 gives an overview of important transporter proteins in the enterocyte. Glucose is actively transported against its chemical gradient into the epithelial enterocytes by cotransport of sodium in SGLT1 (61, 97). Galactose can also bind to SGLT1 in the same way as glucose. Fructose enters by facilitated diffusion through GLUT5. The sodium concentration inside the enterocyte ($[Na_c]$) is kept low by basolateral Na-K-ATPase, which cleaves ATP to transport sodium ions against their concentration gradient out of the cell and potassium ions against their gradient into the cell (23, 67). The sodium concentration in the intestinal chyme ($[Na_m]$) is roughly the same as in extracellular fluid and plasma, i.e., ~140 mM. This is much higher than the concentration inside the enterocytes, i.e., ~50 mM (23). K channels give the basolateral membrane a high K permeability, thus providing a return path for the potassium ions that are imported into the cell by Na-K-ATPase. This allows the absorption of nutrients to continue without a buildup of positive ions (28, 67). The imported glucose, galactose, and fructose are transported out of the enterocytes and into the serosal extracellular area by GLUT2 (52, 81), except for the part of it that is metabolized by the enterocyte. Movement of galactose and fructose is always favorable as their concentrations in blood are low (they are swiftly taken up by the liver). The cotransport of glucose through SGLT1 is utilized to up-concentrate glucose in the enterocyte so that it also can diffuse through GLUT2 into the extracellular area and further into the capillaries.

Whereas nonabsorbing enterocytes have a cylindrical form, the presence of glucose or amino acids cause the basolateral part of the enterocytes to shrink, so that it forms a truncated cone, as shown in Fig. 1. By doing this the enterocytes open up intercellular spaces, which are claimed to increase fluid and nutrient uptake (61–63). The intercellular spaces make it possible for large fluxes to flow without having to pass the less permeable nuclei and mitochondria in the lower part of the enterocyte. In this work we have used the spatial dimensions of rat enterocytes in absorbing state (see *Spatial Dimensions of an Absorbing Enterocyte*).

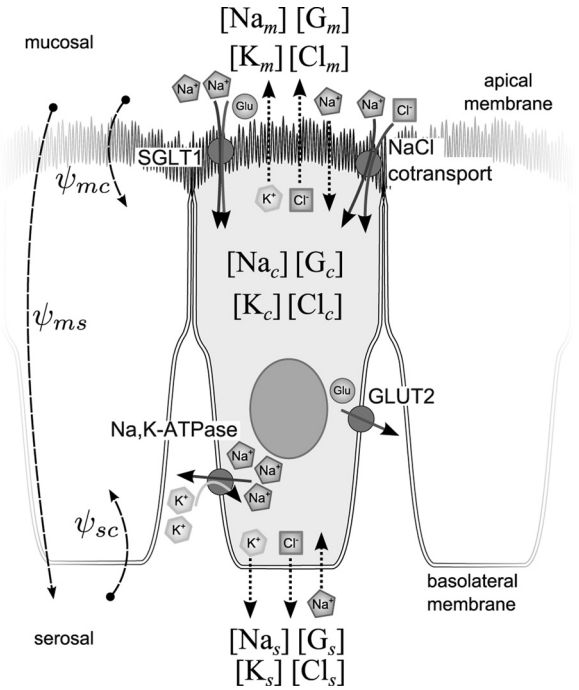

Fig. 1. Epithelial enterocytes in absorbing state. Subscripts m, c, and s mark mucosal, cell inside, and serosal concentrations. SGLT1 absorbs glucose from the intestinal lumen on the apical side of the enterocyte. GLUT2 transports glucose from the cell into the extracellular space on the basolateral side, where the glucose diffuses into capillaries. The absorption of glucose is driven by a sodium gradient maintained by basolateral Na-K-ATPase. Additional sodium enters together with chloride by a coupled flow. Ions also diffuse in and out of the enterocyte (dotted arrows) and directly from the mucosal to the serosal space through paracellular tight junctions between the enterocytes (paracellular flow is not shown in the figure). The arrows point in the normal direction of each flow, which may not be the same as the positive defined direction in our flow expressions. ψ_{mc} is the membrane potential between the mucosal side and the cell inside, ψ_{sc} is the membrane potential between the serosal side and the cell inside, and ψ_{ms} is the transepithelial potential from the mucosal to the serosal side. The apical membrane consists of several microvilli, called the brush border, which greatly increases the effective membrane area where nutrient uptake can occur.

METHODS: MATHEMATICAL MODELING

To provide more insight into the modeling process, we include a short review of the important aspects for each of the transporter proteins before setting up the mathematical rate expressions.

In our modeling, we have followed the principle that all parameters should be identifiable from experiments reported in the literature. Using rate expressions where the proteins are considered to be in steady state (i.e., we do not consider dynamic distribution of different conformations of the same protein) keeps the mathematical model on a moderate level of complexity.

SGLT1

The SGLT1 cotransporter is responsible for the active uptake of glucose from digested food, and it is primarily expressed on the apical, brush border, membrane of intestinal epithelial enterocytes

(97, 99). SGLT1 works by undergoing a cycle of conformational changes, translocating its binding site from the outside to the inside of the cell.

From the work done by Wright and others the kinetics and rate of SGLT1 transport is well known (37, 64, 65, 97). The saturated stoichiometry of the SGLT1 cotransporter is two Na^+ ions for each glucose molecule (31, 64). Studies by Wright et al., revised in Ref. 97, have shown that the flow of glucose and Na^+ through SGLT1 can be adequately described by a cotransport carrier model with six states and ordered binding (65, 97) (see Fig. 2). The model, first introduced by Parent et al. in 1992 (65), describes each subreaction by its corresponding forward and reverse rates. At the outer (mucosal) face, the empty carrier binds first to two Na^+ ions, modeled as one step, and then to one glucose molecule. On the inner (cell) face, glucose is released before Na^+ (last in first out). In the model the empty carrier is assumed to have a charge of -2, making the carrier neutral when bound to two Na^+ ions. The translocation of the empty carrier across the membrane and the binding/release of Na^+ on either sides are thus the only steps that are dependent on the membrane potential.

Parent et al. do not use the normal assumption of rapid equilibrium in their solution of this six-state model. Instead they describe the seven reaction steps by their individual rate constants and derive the steady-state equation for the current through SGLT1 by assuming steady state in the distribution of the different carrier states; the distribution is estimated by employing the King-Altman procedure (65). We use an expression based on the results from Ref. 65 to describe the flow of Na^+ through SGLT1:

$$J_{Na}^{SGLT} = -\frac{2n_{SGLT}}{1.672\cdot 10^{14}}\left(\frac{\varepsilon[Na_m]^2[G_m] + \varphi[Na_m]^2 + \gamma}{\alpha + \beta[G_m] + \chi[Na_m]^2 + [Na_m]^2[G_m]}\right) \quad (1)$$

The expression in the parenthesis, from *Eq. A21* in Ref. 65, is the number of cycles from state 6 to state 1 per second (clockwise direction positive in Fig. 2). The macroconstants α, β, χ, ε, φ, and γ are functions of the rate constants, the concentration of intracellular Na^+ ($[Na_c]$), intracellular glucose ($[G_c]$), and the membrane potential (ψ_{mc}); the expressions are too long to be given here, but they are all listed in *Eqs. A22-A28* in Ref. 65. The flow of Na^+ is two times the number of cycles (we assume no Na^+ leakage, i.e., k_{25} and k_{52} in Fig. 2 are zero) multiplied with the number of SGLT1 transporter proteins situated in the membrane, n_{SGLT}. The division by $1.674\cdot10^{14}$ is used to convert from number of Na^+ ions transported per second to the flow J_{Na}^{SGLT}, which is expressed in μmol/h. The minus sign is included because we define the inward transport as positive (counterclockwise direction positive in Fig. 2).

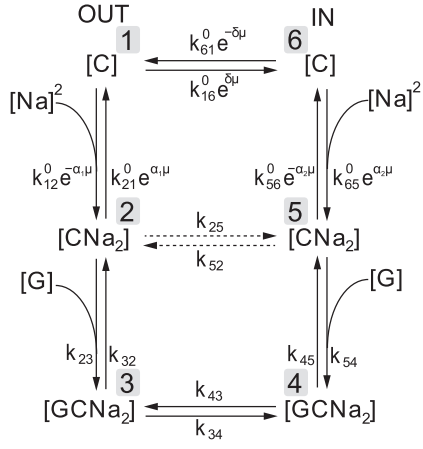

Fig. 2. Six-state kinetic model for SGLT1 first introduced in Ref. 62. The empty carrier has a charge of -2; this means that steps to or from state 1 and 6 may be dependent on the membrane potential. α_1 and α_2 are phenomenological constants that describe the fraction of the electrical field sensed by the Na^+ binding. δ is the fraction of the electrical field sensed by the empty ion binding sites on the carrier during membrane translocation. μ is the electrochemical potential $F\psi_{mc}/RT$. F, R, and T are the Faraday constant, the gas constant, and the temperature, respectively. We have used rate constants from Ref. 97 but with no leakage, i.e., k_{25} and k_{52} are set to zero. The values of the rate constants are listed in Table A2.

Parent et al. (64, 65) originally estimated the rate constants by using iterative numerical simulations of the model adapting it to measured steady-state and presteady-state currents. Experiments done on individual partial reactions in the model have refined these estimates (14, 29, 47). We have used the most recent set of rate constants reviewed in Ref. 97 but have for simplicity not included the transport of Na^+ without glucose ($k_{25} = k_{52} = 0$; see also Table A2). The transition from state 2 to state 3 has a high affinity for glucose, $k_{23} = 45{,}000\ M^{-1}\cdot s^{-1}$, leaving very little carrier available for direct translocation from state 2 to 5. In addition, the translocations from state 2 to 5 and vice versa are very slow; k_{25} and k_{52} are in Ref. 97 reported to have values of only 0.01 s^{-1} and 0.0005 s^{-1}, respectively.

The transport rate of the SGLT1 transporter is relatively low, around one to three full cycles per second. According to the rate constants (97), this is caused by a very slow disassociation of Na^+ at the inner side; k_{56} is only 5 s^{-1}. The low rate means that there has to be a considerable amount of SGLT1 to account for the reported SGTL1-mediated uptake (60). We have estimated the number of SGLT1 transporters in a single rat enterocyte to be in the area of 100–250 million (see *Estimation the Amount of SGLT1*).

Na-K-ATPase

The Na-K-ATPase, also known as the sodium-potassium pump, is a transporter protein that is expressed ubiquitously in cell membranes of higher eukaryotes (20, 23). It is important for maintaining the Na^+ gradient, which drives the apical absorption of glucose in SGLT1. Under normal in vivo conditions, it is established that one pump cycle extrudes three Na^+ ions and takes in two K^+ ions consuming one ATP molecule (23, 66). In intestine epithelial cells, the Na-K-ATPase is primarily found at the serosal side in the basolateral membrane (23, 24, 79).

Our modeling is based on experimental data from the comprehensive work done by Gadsby and Nakao (19, 54), in which they studied the flows of ions through the Na-K-ATPase as electrical currents. At normal in vivo concentrations with no addition or direct control of intracellular K^+, intracellular Na^+ at 50 mM, intracellular ATP at 10 mM, external Na^+ at 150 mM, and external K^+ at 5.4 mM, the turnover rate (cycles per time unit) of Na-K-ATPase is sigmoid shaped with low turnover at negative membrane potential and high turnover at positive membrane potential (19). The turnover rate for one single transporter protein at saturated membrane potential (+40 mV) is roughly 55 s^{-1}, corresponding to a transport of 165 Na^+ ions and 110 K^+ ions per second. We will refer to the above concentrations as base conditions throughout the rest of the article. In our model we describe this voltage-dependent turnover with the function $V^{NaK}(\psi_{sc})$, where ψ_{sc} is the membrane potential between the serosal side and the inside of the enterocyte. In our calculations, $V^{NaK}(\psi_{sc})$ is a polynomial fitted to the experimental data from Gadsby and Nakao (19) (see Fig. A2 in the APPENDIX).

Studies (54) on the change in turnover rate under different internal concentration of Na^+ ions revealed that down to a concentration of 25 mM, the change could be well described with a saturation term multiplied with the voltage-dependent turnover $sat([Na_c])\cdot V^{NaK}(\psi_{sc})$. With the turnover rate at $\psi_{sc} = 0$ mV, and the base conditions described above as reference, a change in internal Na^+ concentration scales the turnover-membrane potential relationship with a value given by the Hill-type saturation: $1.13\cdot[Na_c]^{1.36}/[(K_{0.5}^{Na_c})^{1.36} + [Na_c]^{1.36}]$, where $[Na_c]$ is the intracellular concentration of Na^+ and $K_{0.5}^{Na_c} = 10$ mM. The number 1.13 is an adjustment factor to normalize the value at base conditions with an internal Na^+ concentration of 50

mM. Likewise, a change in external K^+ was found to scale the turnover with: $1.3\cdot[K_s]/(K_{0.5}^{K_s} + [K_s])$, where $[K_s]$ is the serosal concentration of K^+, and $K_{0.5}^{K_s} = 1.5$ mM (54). Also here the number 1.3 is an adjustment factor to normalize the value at base conditions.

Gadsby and Nakao also tested the effect on changing the extracellular Na^+ concentration. The results of these tests indicate that the turnover rate increases at low external Na^+, especially at very negative membrane potentials (ψ_{sc}). This has not been taken into account in our flow expression for the Na-K-ATPase since we intend to operate with constant serosal Na^+ concentrations around 140–150 mM, which are normal in vivo (23).

Assuming that the enterocytes are saturated with ATP, the total rate expression used in our

$$J^{NaK} = V^{NaK}(\psi_{sc}) \cdot n_{NaK} \cdot \frac{1.13[Na_c]^{1.36}}{(K_{0.5}^{Na_c})^{1.36} + [Na_c]^{1.36}} \cdot \frac{1.3[K_s]}{K_{0.5}^{K_s} + [K_s]} \quad (2)$$

where ψ_{sc} is the membrane potential from the serosal side and into the cell. The parameter n_{NaK} is the number of Na-K-ATPase transporter proteins in the cell membrane, and $K_{0.5}^{Na_c}$ and $K_{0.5}^{K_s}$ have the values indicated above. The transport of Na^+ and K^+ through the Na-K-ATPase is three and two times J^{NaK}, respectively.

To the authors' knowledge there exists little data on the amount of Na-K-ATPase in enterocytes. In rabbit kidney cells, the amount is reported to be in the range of 3–50 million (34). Due to similarities in cell function, this range may also be representative for enterocytes.

Coupled Sodium Chloride Inflow

Experimental data have shown that a considerable amount of the total Na^+ and Cl^- inflows across the brush border of rabbit ileum are mediated by a mechanism that behaves as an obligatory one-for-one process, providing electroneutral transport of equal amounts of Na^+ and Cl^- (55). Early studies done by Nellans, Schultz, and others suggested that this inflow was mediated by a NaCl cotransporter (16, 18, 55, 56), but later studies provided evidence that linked this flow to the combined functioning of a Na^+/H^+ exchange and a Cl^-/HCO_3^- exchange process (15, 33, 40, 41).

Although a most complete description would be to model both the Na^+/H^+ exchanger (27, 92, 100) and the Cl^-/HCO_3^- exchanger (24, 94), we have modeled the coupled flow of NaCl by a cotransporter carrier model proposed by Nellans et al. (55). This model assumes that Na^+ and Cl^- are transported together by a single carrier protein and only describes the NaCl part of the flow, i.e., H^+ and HCO^- are not considered. Such a description is adequate for usage in our enterocyte model since we do not include H^+ and HCO_3^-.

The theoretical basis behind the model proposed by Nellans et al. (55) is a general cotransporter carrier model with random binding. Rapid equilibrium is assumed in the model and the translocation steps are considered to be rate limiting (55). For a general expression of the net flow in such a model we direct the reader to Refs. 21 and 49.

Instead of using the complete general expression, Nellans et al. (55) showed that a simplified expression did describe the flow very well. They showed that the inflow was not significantly different if the tissue had been preincubated in either 140 mM NaCl, giving an internal cell concentration of 50 mM Na^+ and 60 mM Cl^-, or 0 mM NaCl. Arguing that the lack of transeffects asserted on the inflow by the internal concentrations of Na^+ and Cl^- suggest that the disassociation on the cell inside is so fast that it does not contribute significantly to alter the inflow of ions per time unit, they proposed an expression on the form (55):

$$J^{NaCl} = \frac{2V_{max}^{NaCl}([Na_m][Cl_m] - [Na_c][Cl_c])}{2K_1K_3 + K_3[Na_m] + K_4[Cl_m] + 2[Na_m][Cl_m]} \quad (3)$$

We use this expression in our model, where the K parameters have the same values as used by Nellans et al. $K_1 = 14$ mM, $K_3 = 22$ mM, and $K_4 = 56$ mM. Since the coupled flow of Na^+ and Cl^- is linked to the combined functioning of more than one transport protein, we have not separated out a parameter for the number of NaCl transporting entities. V_{max}^{NaCl} is hence a parameter describing the maximum flow of coupled NaCl transport for the whole enterocyte.

It should be noted that Nellans et al. (55) based this expression on unidirectional inflow measurements alone. The lack of internal concentrations in the denominator corresponds to a fast disassociation on the cell inside, so fast that it does not contribute significantly to alter the inflow of ions per time unit. However, the unidirectional outflow may be markedly dependent on the internal concentrations. This suggests that the expression we use for the net flow in *Eq. 3*, which relies on the argument from Nellans et al., is only reasonable as long as the unidirectional inflow is dominating, i.e., there is a net inflow. This is the case when $[Na_m][Cl_m] > [Na_c][Cl_c]$, which we have in all our simulations.

GLUT2

The glucose absorbed into the enterocytes from the lumen is transported out of the enterocytes by facilitated diffusion through GLUT2 transporter proteins that are situated in the basolateral membrane (81). The glucose exits to the extracellular serosal space near blood capillaries.

The kinetics of GLUT2 in enterocytes was examined by Maenz and Cheeseman (52), who used isolated cells and purified basolateral vesicles from rat small intestine to measure kinetic parameters for glucose transport through GLUT2 in both directions (inflow into glucose empty vesicles, and outflow into glucose free media). Maenz and Cheeseman found that GLUT2, in enterocytes, is kinetically asymmetric with an inward half saturation constant of 48 mM and an outward half saturation constant of 23 mM. The maximum flow was also found to be asymmetric with a fivefold higher rate into than out of the enterocyte, i.e., 1,138 and 203 $pmol\cdot s^{-1}\cdot mg$ basolateral membrane $protein^{-1}$, respectively. The asymmetric identity is associated with the orientation of the membrane inserted GLUT2 protein. Asymmetric behavior is reported for several of the other members from the SLC2 family (82), e.g., asymmetric transport of sugars through GLUT1 in human red blood cells (3).

To model the flow of glucose through GLUT2 we use an expression based on the so-called fixed-site carrier model, suggested by Baker and Widdas (3). This model treats the transporter protein as a pore with two binding sites, one on the inward facing side (c) and one on the outward facing side (s). The net flow from the inside to the outside of the cell is then given as

$$J^{GLUT} = \frac{V_{max}^{G_c}K_{0.5}^{G_s}[G_c] - V_{max}^{G_s}K_{0.5}^{G_c}[G_s]}{(K_{0.5}^{G_c} + [G_c])(K_{0.5}^{G_s} + [G_c])} \cdot n_{GLUT} \quad (4)$$

where $V_{max}^{G_c}$ and $V_{max}^{G_s}$ are the maximum transport rate out of and into the enterocyte for one single GLUT2 transporter. $K_{0.5}^{G_c}$ and $K_{0.5}^{G_s}$ are the half saturation constants for the inside facing and the outside facing binding sites, respectively. $[G_c]$ and $[G_s]$ are the concentrations of glucose inside and outside of the enterocyte, respectively, and n_{GLUT} is the number of GLUT2 transporter proteins in the basolateral membrane.

At zero-trans conditions this rate expression reduces to a Michaelis-Menten form, hence making the constants easy identifiable from the studies of Maenz and Cheeseman (52). However, we had to make some adjustments of the parameters to ensure zero net flow at equal concentrations, in keeping with the Haldane relationship, $V_{max}^{G_c}K_{0.5}^{G_s} = V_{max}^{G_s}K_{0.5}^{G_c}$. These adjustments are discussed in *Adjustment of Kinetic Parameters for GLUT2*.

Diffusive Flows

Diffusive flows of Na^+, K^+, and Cl^- are also included in our model. We use the Goldman-Hodgkin-Katz (GHK) flux equation (70)

to describe the diffusive flows across the apical and the basolateral membrane. The equation has the form:

$$J_i^{\mathrm{D}} = -\frac{P_i z_i F\psi}{RT}\left(\frac{[i_{\mathrm{out}}] - [i_{\mathrm{in}}]\exp(z_i F\psi/RT)}{1-\exp(z_i F\psi/RT)}\right)\cdot A \qquad (5)$$

The subscript i denotes the ion (Na^+, K^+, or Cl^-), P_i is the membrane permeability of ion i, z_i is the valence of the ion, $[i_{\mathrm{out}}]$ and $[i_{\mathrm{in}}]$ are the outer and inner concentrations of the ion, and ψ is the membrane potential (ψ_{mc} for the apical and ψ_{sc} for the basolateral membrane). F, R, and T are the Faraday constant, the gas constant, and the temperature, respectively. The GHK flux-equation gives the diffusive flow as a flux, i.e., flow per membrane area, so we multiply with the membrane area A (see Table A2) to find the total diffusive flow over the membrane. The diffusive flows given by *Eq. 5* are positive when directed into the cell.

The permeability coefficients account for the total diffusive flow, including diffusion through ion channels. The most notable type of ion channels in enterocytes is the basolateral K channels (28, 86). The K channels give the enterocyte a high permeability for K^+ and provide a return path for the K^+ ions imported into the cell by the Na-K-ATPase. Regulation of the K permeability also plays an important part in the ionic homeostasis in enterocytes. This is further discussed in *Regulation of basolateral K permeability and potassium homeostasis*.

In addition to diffusive flows into the cell, we also include diffusive paracellular flows that allow ions to travel directly from the mucosal to the serosal side through the tight junctions. These paracellular flows are calculated by *Eq. 5*, using the mucosal concentration of the ion as the outer concentration and the serosal concentration as the inner concentration and ψ_{ms} as the membrane potential from the mucosal to the serosal side. The paracellular flows are positive when directed from the mucosal to the serosal side.

Cell Membrane Potential

The SGLT1 and the Na-K-ATPase are both electrogenic transporters, i.e., the transport of ions through these proteins constitute electrical currents flowing in and out of the enterocyte. Diffusive ion flows are also electrical currents, and this, together with the fact that the flows are driven by processes that are dependent on the membrane potential, makes it essential to include the membrane potential of the enterocyte in our model.

Our enterocyte model includes the mucosal to cell (apical) membrane potential ψ_{mc}, the serosal to cell (basolateral) membrane potential ψ_{sc}, and the potential over the whole epithelial layer from mucosal to serosal ψ_{ms}, see Fig. 1. Only two of these are independent as the potentials are related by the equation:

$$\psi_{\mathrm{ms}} = \psi_{\mathrm{mc}} - \psi_{\mathrm{sc}} \qquad (6)$$

An important principle for any form of transport of ions into and out of cells is the principle of electroneutrality (42, 70), which states that the bulk or macroscopic concentrations of positive and negative ions has to be equal at all times. The reason behind this principle is that only a very small amount of charge separation is needed to create a large electric field. A charge difference of 1 mM more positively charged ions than negatively charged ions will for a cell with the dimensions used in this work (see *Spatial Dimensions of an Absorbing Enterocyte*) give an electric field inside the membrane with a magnitude of about $2{\cdot}10^9$ V/m. With this field strength and a membrane thickness of 7.5 nm (77), the corresponding membrane potential is in the order of 10 V/meq of charge difference. Thus a membrane potential in the range of millivolts corresponds to a negligible difference in concentration, which is too small to be measured by most chemical methods (42).

Cell electroneutrality holds when there is no net current into the cell, i.e.

$$\sum_i z_i\left(J_i^{\mathrm{a}} + J_i^{\mathrm{bl}}\right) = 0 \qquad (7)$$

where J_i^{a} and J_i^{bl} are the inflow of species i, with valence z_i, over the apical and basolateral membrane, respectively. For the same reasons as above, any buildup of charge on either the mucosal or the serosal side would result in unphysical high values for the transepithelial potential (ψ_{ms}). To preserve mucosal and serosal bath electroneutrality the net epithelial current must thus also be zero,

$$\sum_i z_i\left(J_i^{\mathrm{p}} - J_i^{\mathrm{bl}}\right) = 0 \qquad (8)$$

where J_i^{p} is the paracellular inflow into the serosal space of species i, with valence z_i.

The principle of electroneutrality, in the form of *Eqs. 7* and *8*, is often used as a condition to help calculate the membrane potentials in models of epithelial transport [see for instance Stephenson and Weinstein's models of renal epithelium (87, 93, 96)]. The idea is to compute a value for the membrane potential that, when used to calculate the individual flows, gives a zero net current.

We have chosen to use an iterative approach as outlined in Ref. 43. At each time step we start with guess values for the membrane potentials and calculate the flows; the estimate for the membrane potential is then refined using the Newton-Raphson method and the flows are recalculated until the net cell current (*Eq. 7*) and the net epithelial current (*Eq. 8*) are sufficiently close to zero ($<10^{-9}$ pmol/h). Once the flows are in keeping with *Eqs. 7* and *8* we integrate the net flow of each species over the length of the time step to update the concentrations. This iterative calculation of the membrane potentials is well proven for epithelial models (25, 43, 85). A detailed description of our implementation and validation of the iterative method is given in *Iterative Calculation of Membrane Potentials*.

Integrative Model

We build our model by combining the reaction kinetic expressions for SGLT1, Na-K-ATPase, coupled NaCl inflow, GLUT2, and diffusive flows into a set of nonlinear differential equations, shown in *Model Equations*. As described above the flows are calculated together with the membrane potentials at each time step in the simulation by an iterative method. The model describes the dynamical behavior of flows, as well as the concentration of intracellular chemical species (cell glucose [G_c], cell sodium [Na_c], cell potassium [K_c], and cell chloride [Cl_c]), and the cell membrane potentials (ψ_{mc}, ψ_{sc}, and ψ_{ms}). The model does not consider the amount of glucose metabolized by the enterocyte itself.

The model was implemented and solved numerically by using Matlab/Simulink from MathWorks. Numerical integration of the differential equations is done by the Matlab/Simulink solver *ode23tb*. The solver uses an absolute and relative tolerance of 10^{-6} and a variable time step length between 3.6 and 360 ms. Simulations run quickly on an ordinary desktop computer; it takes about half a minute to simulate a 4-min short-term response to a transient change in mucosal glucose and about a minute to simulate a 40-min long-term response to a stepwise (constant) change in glucose (see *Short-Term Response to Mucosal Glucose* and *Long-Term Response with Controller Motifs*, respectively).

The parameters used are listed in the APPENDIX (see Table A2) and are as discussed based on experimental data and evidence. However, some adjustments of the ionic permeabilities had to be done as we found little usable data on permeability coefficients for enterocytes. Studies exists (4, 17), but they are old and unreliable. Measurements are typically done for whole tissue layers without blocking nondiffusive pathways for active transport and cotransport. For the paracellular permeabilities we started with values reported for rabbit ileum (17), and for the mucosal and serosal membrane we started with permeability coefficients from a Necturus gallbladder model (1). The coefficients were then adjusted by trial and error until reasonable re-

sponses were observed, primarily in the membrane potential. The most prominent adjustments were made in the apical permeability for K^+ (P^a_K), which was reduced to be in the same order of magnitude as the apical permeability for Na^+ (P^a_{Na}) as reported for rat small intestine (4), and the basolateral Na^+ permeability (P^{bl}_{Na}), which was increased since it in Ref. 1 was set to zero. We kept the ratio between the paracellular permeabilities as in Ref. 17 but had to increase the magnitude to reduce the transepithelial potential to ~3 mV as reported in Refs. 59 and 69.

RESULTS

We first tested the short-term behavior of the model, without adding additional regulatory mechanisms for ionic homeostasis. During a short timeframe (up to 5 min), it is reasonable to assume that the amount of transporter protein in the membrane remains constant, as regulation of transporter protein expression by transcriptional and translational pathways may have little influence.

Short-Term Response to Mucosal Glucose

Short-term response to changes in mucosal glucose is well studied in vitro (7, 30, 69), and thus, provides a sound basis for testing our model. We have simulated its response to a short-term increase in mucosal glucose ($[G_m]$) similar to the experimental studies performed on rabbit ileum by Rose and Schultz (69). Mimicking the conditions of Rose and Schultz, we abruptly increase the mucosal glucose concentration from 100 μM to 20 mM and then let it fall back to 100 μM in an exponential manner, as to simulate glucose being flushed out (see Fig. 3*A*). Using parameters from the literature as described in METHODS: MATHEMATICAL MODELING (see Table A2 for list of parameters), the response in state variables from the model is shown in Fig. 3, *B–H*, whereas the flows are shown in Fig. 4.

The simulation shows that the addition of mucosal glucose leads to a less negative mucosal to cell membrane potential

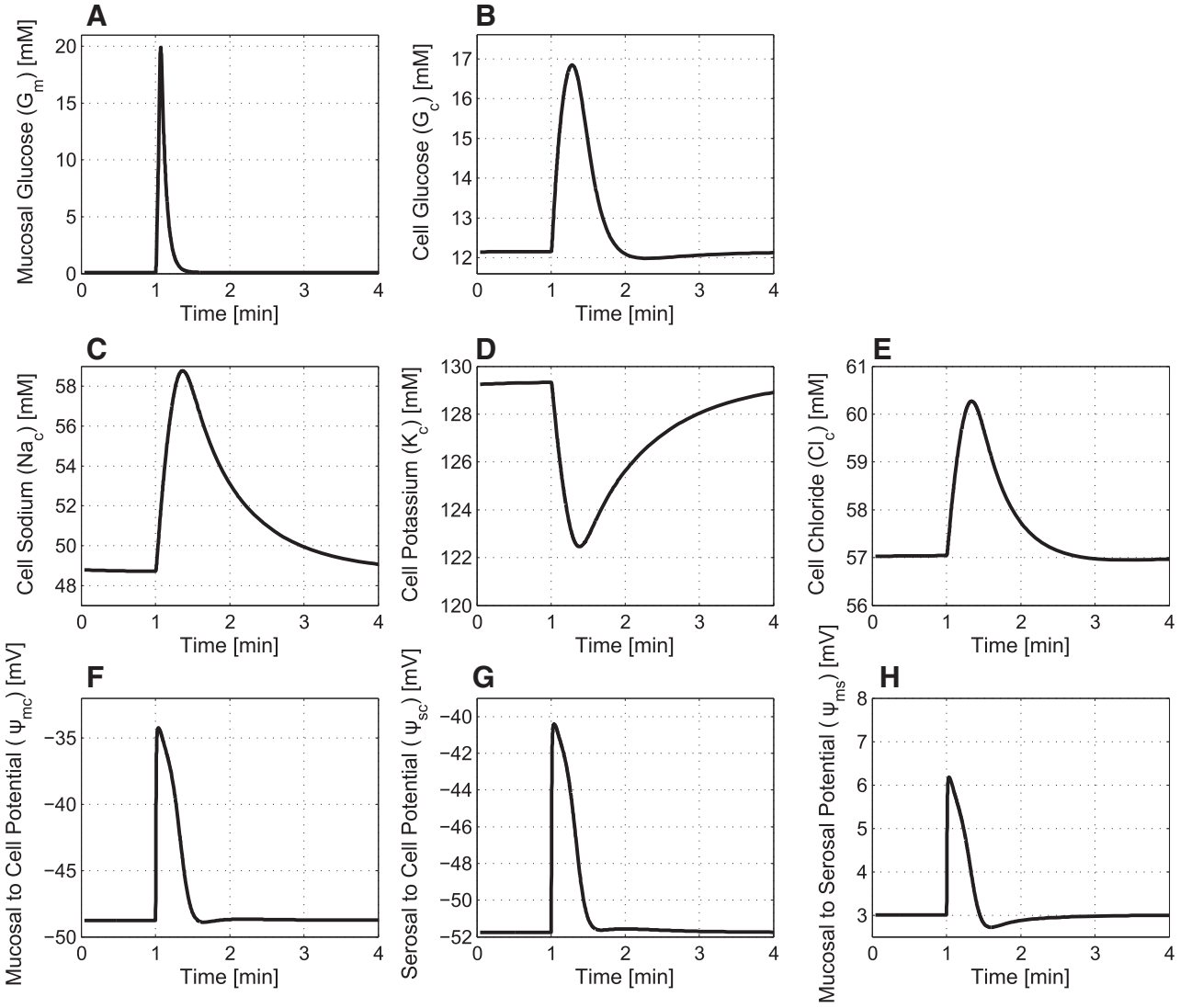

Fig. 3. Simulated model response to a short-term change in mucosal glucose using parameters in Table A2. *A*: at $t = 1$ min, the mucosal side glucose concentration ($[G_m]$) is increased from 100 μM to 20 mM (step). The mucosal side is then flushed with media without glucose (using a flush time of 20 s as in Ref. 69). This gives in an impulse shaped change in $[G_m]$. *B*: cell glucose concentration ($[G_c]$). *C*: concentration of cell sodium ($[Na_c]$). *D*: concentration of cell potassium ($[K_c]$). *E*: concentration of cell chloride ($[Cl_c]$). *F*: mucosal to cell membrane potential (ψ_{mc}). *G*: serosal to cell membrane potential (ψ_{sc}). *H*: mucosal to serosal membrane potential (ψ_{ms}).

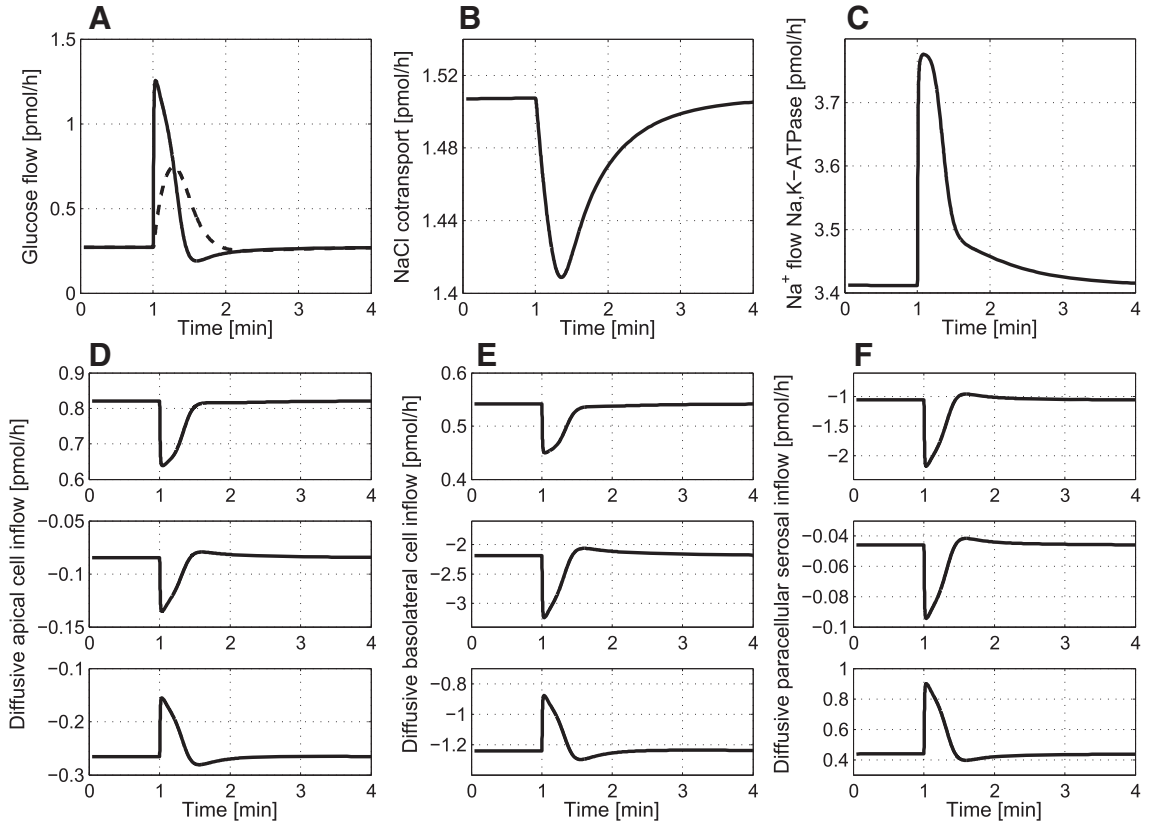

Fig. 4. Simulated model flows during a short-term change in mucosal glucose, using model parameters from Table A2. *A*: glucose inflow through SGLT1 (solid) and outflow through GLUT2 (dashed). *B*: coupled NaCl inflow. *C*: outflow of Na^+ through Na-K-ATPase. *D*: diffusive inflow of Na^+ (*top*), K^+ (*middle*), and Cl^- (*bottom*) over the apical membrane. *E*: diffusive inflow of Na^+ (*top*), K^+ (*middle*), and Cl^- (*bottom*) over the basolateral membrane. *F*: diffusive inflow to the serosal side of Na^+ (*top*), K^+ (*middle*), and Cl^- (*bottom*) through the paracellular junctions (negative inflow is the same as outflow).

(ψ_{mc}; Fig. 3*F*) and a more positive mucosal to serosal membrane potential (ψ_{ms}; Fig. 3*H*), in good agreement with the experimental findings of Rose and Schultz (69). A direct comparison of the simulated membrane potential response and the experimental findings in Ref. 69 is shown in the DISCUSSION (see Fig. 11).

The steady-state levels of cell Na^+, K^+, and Cl^- are in the expected range (55, 57). The short-term increase in cell Na^+ (see Fig. 3*C*) is supported by experiments (30), but is reported to fall over time if the mucosal concentration is kept high instead of being flushed out, indicating a slower regulatory mechanism that increases the number of Na-K-ATPase transporters (30). This is further discussed in *Regulation of Na-K-ATPase and sodium homeostasis*.

The reduced concentration of intracellular K^+ (Fig. 3*D*) is a result of an increased outflow of K^+ (Fig. 4*E*) due to membrane depolarization. The change in membrane potential towards more positive values increases the diffusive K^+ outflow, in agreement with *Eq. 5*. K^+ is removed faster than the Na-K-ATPase imports K^+, a property that is anticipated based on experimental results (7, 22).

Net epithelial flows of Na^+, K^+, and Cl^- are found by summing the basolateral and paracellular flows. Figure 5 shows the net flows during the short-term increase in mucosal glucose. Focusing on the steady state before and after the step in mucosal glucose, we see that Na^+ and Cl^- are absorbed from the intestine, in keeping with enterocytes being Na^+ absorbing epithelia (73). There is a small leak of K^+ in the opposite direction, which is expected because some of the K^+ pumped into the cell at the basolateral membrane will escape through K conductance in the apical membrane (Fig. 4*D*). The rate of K^+ secretion is very low (0.14 pmol/h) compared with the inflow of Na^+ and Cl^- (1.82 and 1.68 pmol/h), ~8% of the Na^+ inflow, and is believed to be of little physiological significance (71). Although there is an increase in Na^+ pumped by the Na-K-ATPase (Fig. 4*C*), the net epithelial Na^+ inflow decreases during the transient phase (Fig. 5*A*). This is caused by the increase in paracellular back flow of Na^+ into the lumen (Fig. 4*F*); a more positive transepithelial potential ψ_{ms} (Fig. 3*H*) drives this paracellular movement of Na^+.

Short-Term Response to Mucosal Na^+

The enterocyte response to short-term changes in mucosal Na^+ is well studied (57, 59, 69). We simulated short-term changes in the concentration of mucosal Na^+ ($[Na_m]$) by changing the mucosal Na^+ from its base value of 140 to 100 mM and back again in a stepwise manner. The concentration of mucosal glucose was kept constant at 0.5 mM. Figure 6 shows the simulated model response. When the mucosal sodium concentration is kept at 100 mM, the model reaches a new steady state; the reduced availability of mucosal Na^+ leads to a decrease in the intracellular Na^+ concentration ($[Na_c]$) (see Fig. 6*A*). The decrease in intracellular Na^+ is balanced by

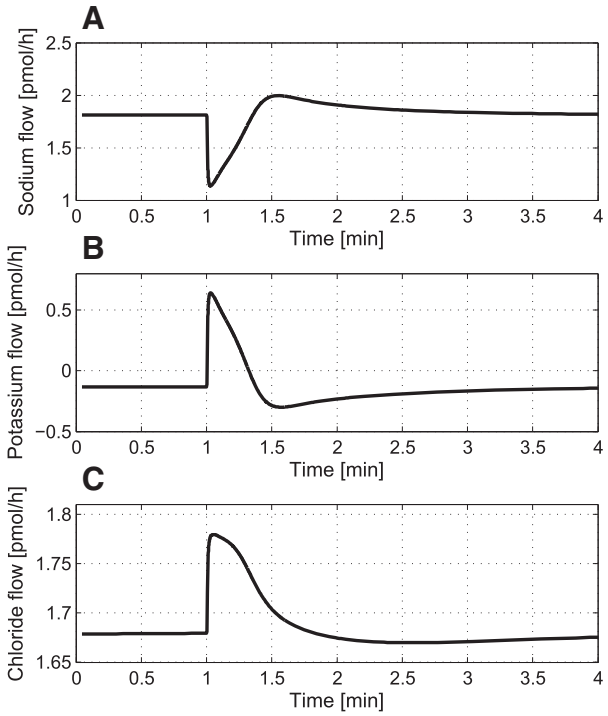

Fig. 5. Simulated net inflows (positive into serosal area) over the epithelial layer; this is the net sum of transcellular and paracellular flows. *A*: inflow of Na^+ ($J_{Na}^{Epi} = 3J^{NaK} - J_{Na}^{Dbl} + J_{Na}^{Dp}$). *B*: inflow of K^+ ($J_K^{Epi} = -2J^{NaK} - J_K^{Dbl} + J_K^{Dp}$). *C*: inflow of Cl^- ($J_{Cl}^{Epi} = -J_{Cl}^{Dbl} + J_{Cl}^{Dp}$).

decrease in intracellular Cl^- (Fig. 6*C*) and an increase in intracellular K^+ (Fig. 6*B*).

The simulation also shows cell hyperpolarization (see Fig. 6, *D–F*) as a result of decreased mucosal Na^+. The reversal of polarity from positive to negative of the transepithelial potential ψ_{ms} is particularly noteworthy. These results are similar to what have been observed in rat duodenum (59). The change in ψ_{mc} and ψ_{ms} of about -6 mV is in the same range as reported for the same change in mucosal Na^+. Changing the mucosal Na^+ concentration back to 140 mM causes the enterocyte to return to its initial state.

There is a continuous net absorbance of Na^+ and Cl^- from the intestine during the whole simulated response to this change in mucosal Na^+. The net inflow of Na^+ goes from 1.86 to 0.85 pmol/h when mucosal Na^+ changes from 140 to 100 mM (results not shown).

Extending the Model to Test Regulatory Mechanisms

Having shown that the enterocyte model behaves as expected for short-term dynamics, we continue to test our hypothesis by adding regulatory mechanisms to the model.

Regulation of Na-K-ATPase and sodium homeostasis. Experiments show that when mucosal glucose is increased and kept high, the increase in intracellular Na^+ ($[Na_c]$) is followed by a slow decrease back to basal values, indicating a mechanism that increases the number of Na-K-ATPase transporter proteins to maintain Na^+ homeostasis (30). This increase may stem from increased synthesis as it has been shown to do in central neurons and cardiocytes (74, 98) or from a cytoplasmic holding area of available Na-K-ATPase proteins (73).

Our hypothesis is that the observed homeostasis can be explained by a production of Na-K-ATPase directly regulated by intracellular Na^+. Intracellular Na^+ has been shown to directly regulate the Na-K-ATPase gene expression in other cell types (74, 98).

We have earlier presented a set of simple controller motifs that can bring about robust homeostasis (10, 83). Because Na-K-ATPase can be said to work as an outflow controller by transporting Na^+ out of the cell, the activating outflow controller (type 5) from our work is a possible candidate for the mechanism that regulates Na^+ by adjusting the number of Na-K-ATPase proteins. The controller motif is shown in Fig. 7.

Our motif treats the concentration of intracellular Na^+ as an activator for the synthesis/insertion of Na-K-ATPase proteins, modeled as a first order process, where the insertion rate is given as $k_{NaK} \cdot [Na_c]$. The degradation (or removal) of Na-K-ATPase is assumed to be similar to an enzymatic process where the degradation enzyme E_{set}^{NaK} is saturated. This controller motif extends the model with the following differential equation:

$$\dot{n}_{NaK} = k_{NaK} \cdot [Na_c] - \frac{V_{max}^{E_{set}^{NaK}} \cdot n_{NaK}}{K_{0.5}^{E_{set}^{NaK}} + n_{NaK}} \quad (9)$$

where $V_{max}^{E_{set}^{NaK}}$ and $K_{0.5}^{E_{set}^{NaK}}$ are the maximum rate and the half saturation constant for the enzyme/process that removes Na-K-ATPase. Saturation of the Na-K-ATPase removing process ensures regulation of intracellular Na^+ to the setpoint $V_{max}^{E_{set}^{NaK}}/k_{NaK}$, because saturation provides near zero-order kinetics. In detail, the setpoint for intracellular Na^+ is determined by the steady-state condition of *Eq. 9*. With $K_{0.5}^{E_{set}^{NaK}} \ll n_{NaK}$ (saturation) the degradation term is approximately constant at $V_{max}^{E_{set}^{NaK}}$, and thus $\dot{n}_{NaK}$ is zero when $[Na_c]$ is at the setpoint $V_{max}^{E_{set}^{NaK}}/k_{NaK}$. We have previously shown that zero-order kinetics is a sufficient condition for integral control (58). The outflow of Na^+ is still given by the J^{NaK} expression (*Eq. 2*), but the amount of Na-K-ATPase (n_{NaK}) will now change dynamically according to *Eq. 9* to counteract the perturbations in Na^+ inflow. A transient increase in intracellular Na^+ (from increased apical inflow) causes the amount of Na-K-ATPase to increase ($\dot{n}_{NaK} > 0$); this increase continues until the outflow of Na^+ through Na-K-ATPase is so large that the concentration of intracellular Na^+ is brought back down to its setpoint.

Regulation of basolateral K permeability and potassium homeostasis. The pump-leak parallelism between K permeability and the stimulation of basolateral Na-K-ATPase is well studied (7, 28, 73). An increase in the Na-K-ATPase pump rate, as seen under the uptake of nutrients, is accompanied by an increase in the basolateral K permeability. Whether this increase stems from an increased expression of K channels or from nontranscriptional mechanisms is not yet fully understood as little is known about changes in K-channel expression in enterocytes (28).

Most works have focused on elucidating nontranscriptional regulation and one prominent feature is an apparent Ca^{2+} activation of the K channels (75). Other nontranscriptional regulatory mechanisms include activation by cell swelling, membrane stretch, and also an interesting inverse dependence on cytosolic ATP (28, 84).

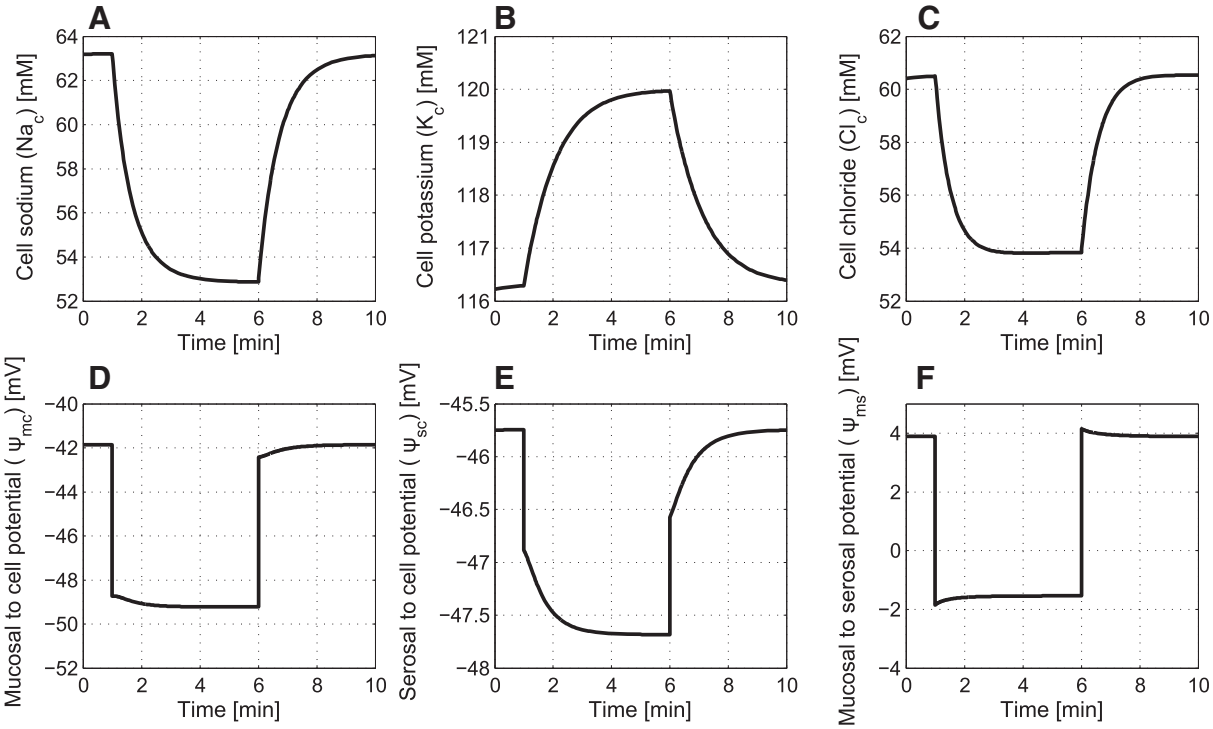

Fig. 6. Simulated model response to a short-term change in mucosal sodium using model parameters in Table A2. At $t = 1$ min, the mucosal side Na^+ concentration ($[Na_m]$) is decreased from 140 to 100 mM (step), and at $t = 6$ min, the Na^+ concentration is changed back to 140 mM. *A*: cell sodium concentration ($[Na_c]$). *B*: concentration of cell potassium ($[K_c]$). *C*: concentration of cell chloride ($[Cl_c]$). *D*: mucosal to cell membrane potential (ψ_{mc}). *E*: serosal to cell membrane potential (ψ_{sc}). *F*: mucosal to serosal membrane potential (ψ_{ms}).

Our attention in this work is on the regulation of K permeability by intracellular ATP. Basolateral K_{ATP} channels have been found in enterocytes (12) and other epithelia (84). The increased usage of ATP by Na-K-ATPase during absorption lowers the intracellular concentration of ATP; this reduction in intracellular ATP relieves the inhibition of basolateral K_{ATP} channels, thus increasing the K permeability.

Structuring this into a controller motif we have that intracellular ATP acts as an outflow controller of $[K_c]$ (see Fig. 8). ATP is used by the Na-K-ATPase at a rate of J^{NaK}. We assume that the synthesis of ATP can be modeled by an expression on the form $k_1^{ATP}\{K_{0.5}^{ATP}/(K_{0.5}^{ATP} + [ATP])\}$, i.e., that the synthesis of ATP increases when the concentration of ATP decreases. The theoretical maximum rate of synthesis is k_1^{ATP} when [ATP] is zero, and $K_{0.5}^{ATP}$ is the concentration of ATP where the rate of synthesis is half of k_1^{ATP}. The synthesis of ATP must increase as the concentration of intracellular ATP is reduced to reach a new steady state, otherwise an increase in J^{NaK} would simply deplete the cell of ATP as the synthesis would never catch up with the increased consumption.

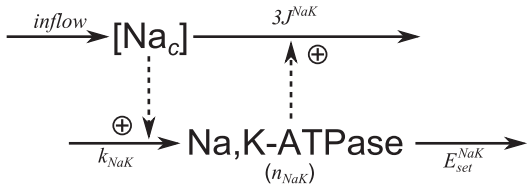

Fig. 7. Controller motif proposed for the regulation of intracellular Na^+ by production of Na-K-ATPase.

The inverse relation between the concentration of intracellular ATP and current through K_{ATP} channels has been quantified in cardiac myocytes (35). The current through the K channels is inhibited by [ATP] with an inhibition constant K_I^{ATP} of 0.8 mM. From this basis we express the relationship between ATP and basolateral K permeability on a standard inhibition form as: $P_K^{bl} = P_{Kmax}^{bl} K_I^{ATP}/(K_I^{ATP} + [ATP])$. By doing this we end up with a slightly modified controller motif of type 6 (see Ref. 10). The degradation of the controller species, which is intracellular ATP, is proportional to the inflow, rather than the concentration, of the controlled species $[K_c]$.

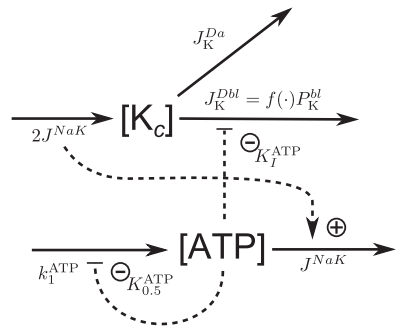

Fig. 8. Controller motif proposed for the regulation of intracellular K^+. The degradation of ATP is coupled to the pump rate of the Na-K-ATPase. ATP affects the basolateral permeability to K^+ by inhibiting the K channels, working as an outflow controller of $[K_c]$. ATP also inhibits its own synthesis.

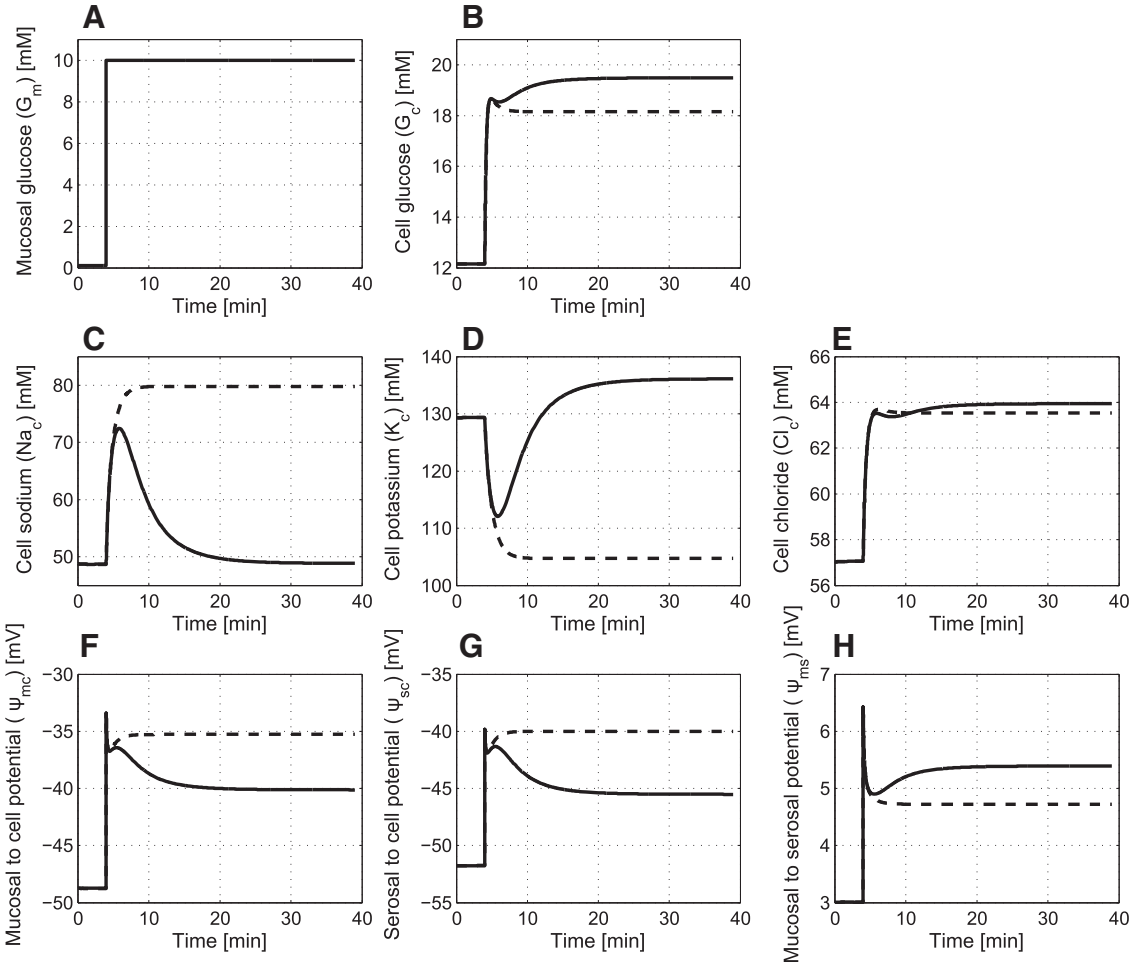

Fig. 9. Simulated model response to long-term change in mucosal glucose (solid lines) using model parameters in Table A2. The motif parameters are fitted to achieve a setpoint for intracellular sodium at ~49 mM, a setpoint for intracellular potassium at ~130 mM, and a reasonable dynamic response (10). For reference, we have also included the results from simulating the model without the 2 regulatory mechanisms (dashed lines). *A*: at time $t = 4$ min mucosal glucose concentration ([G_m]) is stepped from 0.1 to 10 mM. *B*: cell glucose ([G_c]). *C*: cell sodium ([Na_c]) *D*: cell potassium ([K_c]). *E*: cell chloride ([Cl_c]). *F*: mucosal to cell membrane potential (ψ_{mc}). *G*: serosal to cell membrane potential (ψ_{sc}). *H*: mucosal to serosal membrane potential (ψ_{ms}).

This controller motif leads to a differential equation describing the dynamics in [ATP], and an expression for the basolateral K permeability as

$$\dot{[\mathrm{ATP}]} = \frac{1}{V_c}\left(k_1^{\mathrm{ATP}}\frac{K_{0.5}^{\mathrm{ATP}}}{K_{0.5}^{\mathrm{ATP}} + [\mathrm{ATP}]} - J^{\mathrm{NaK}}\right) \qquad (10)$$

$$P_{\mathrm{K}}^{\mathrm{bl}} = P_{\mathrm{Kmax}}^{\mathrm{bl}}\left(\frac{K_{\mathrm{I}}^{\mathrm{ATP}}}{K_{\mathrm{I}}^{\mathrm{ATP}} + [\mathrm{ATP}]}\right) \qquad (11)$$

where V_c is the cell (cytoplasm) volume and $K_I^{ATP} = 0.8$ mM. P_{Kmax}^{bl} can be found from P_K^{bl} and the steady-state level of [ATP], which is ~4.3 mM in enterocytes (9). We have adjusted k_1^{ATP} so that [ATP] is in steady state (4 mM in our simulations) before the addition of nutrients; K_I^{ATP} is set to 0.5 mM.

Long-Term Response with Controller Motifs

Adding these two controller motifs to the model gives the long-term responses shown in Figs. 9 and 10 (solid lines) for a stepwise increase in mucosal glucose (note the time scale). The results show adaptation in the concentration of intracellular Na^+ (Fig. 9*C*) and K^+ (Fig. 9*D*) where the concentrations are regulated towards their setpoints of ~49 and 130 mM, respectively. Comparing this to the simulation results of an enterocyte without the regulatory mechanisms (dashed lines in Fig.

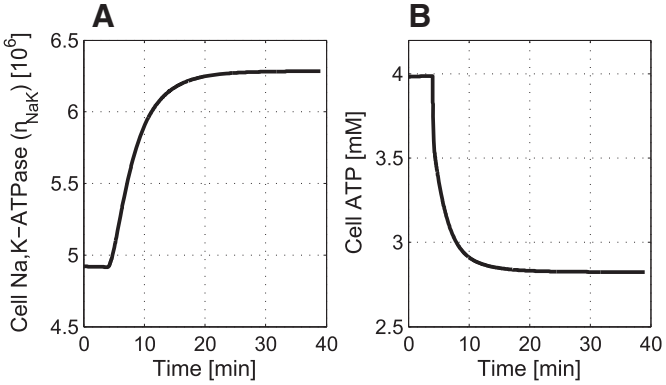

Fig. 10. Simulated model response to long-term change in mucosal glucose using model parameters from Table A2. *A*: amount of Na-K-ATPase (n_{NaK}). *B*: concentration of ATP ([ATP]).

9), which has no adaptation at all, shows how much is gained by these motifs.

The adaptation is not perfect in the sense that exactly the same ionic concentrations are achieved before and after the step; the concentration of K^+ is for instance close to 129 mM before the step in mucosal glucose and 136 mM after the step. There is a slight overadaptation (11) (Fig. 9*D*). This has to do with the accuracy of the controller motif for intracellular K^+ (10). As expected there is no adaptation in the concentration of Cl^- (Fig. 9*E*), as there is no specific controller motif regulating Cl^-.

The amount of Na-K-ATPase and ATP is shown in Fig. 10. The reduction in ATP from 4 to 2.8 mM fits well with reported values for absorbing epithelial cells in the renal proximal tubule (84).

In addition to maintaining the ionic concentration at their setpoints, the regulation also enables a higher total flow through the enterocyte (data not shown). The net epithelial flow of Na^+ increases by 20% after the step in mucosal glucose with regulation (from 1.8 to 2.2 pmol/h) whereas it without regulation only increases by 5% (from 1.8 to 1.9 pmol/h). The net flow of glucose is 13% higher with regulation than without.

The results also show a hyperpolarization of the membrane potential compared with the situation with no regulation (Fig. 9, *F–H*). The transepithelial potential (ψ_{ms}) increases with the step in mucosal glucose and is higher with regulatory motifs than without. This fits with the higher total ionic flow from mucosal to serosal with regulation.

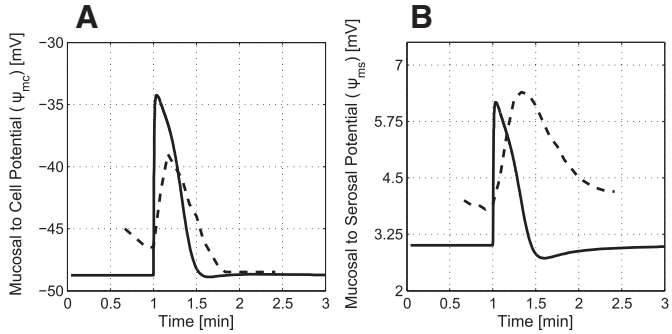

Fig. 11. Simulated model response in membrane potential (solid) and replotted experimental values (dashed). [Reprinted from Rose and Schultz (69) with permission.] At $t = 1$ min the mucosal side glucose concentration ($[G_m]$) is increased from 10 μM to 20 mM (step). The mucosal side is then flushed so that it falls back to 10 μM (using a flush time of 20 s). *A*: mucosal to cell potential ψ_{mc}. *B*: mucosal to serosal potential ψ_{ms}.

DISCUSSION

We asked whether the available kinetic data could be combined to form a mathematical model of glucose absorption in enterocytes and whether such a model could be used to predict regulatory mechanisms for ionic homeostasis in enterocytes. More specifically, we wanted to test whether regulation of Na-K-ATPase by intracellular Na^+ together with an ATP-based regulation of the basolateral permeability for K^+ could explain how enterocytes adapt to changing inflow of Na^+.

Model and Short-Term Response

The short-term response of our model shows that the modeled enterocyte behaves as expected from experiments reported in literature. This confirms that reaction rates, and other results, from studies done on *specific* enterocyte transporter proteins in isolation can be combined to form an *integrated* model that describes the transport of glucose, and the cell homeostasis of ions, in a satisfactory manner.

Figure 11 shows the membrane potential response from our simulated change in mucosal glucose (from Fig. 3) together with the experimental data from the study by Rose and Schultz (69) on rabbit ileum. In our view the match is remarkable considering the fact that most of our parameters are gathered from the literature of single transporter type studies, done with proteins from different organisms including human type SGLT1 expressed in oocytes (97), guinea pig Na-K-ATPase from ventricular myocytes (19, 54), and GLUT2 from rat enterocytes (52). The spikier simulated response in membrane potential (Fig. 11) may be related to the effect of unstirred layers around the microvilli. A gradual equilibrating between the mucosal bath and the microvilli area will effectively drag out the response.

Because our kinetic flow expressions and physiological parameters are based on single transporter type studies, parameter fitting would probably be needed if we were to evaluate the model's ability to exactly match quantitative results from studies done on whole enterocytes. Cell variance would in that case also have to be considered, e.g., the membrane potential of rabbit enterocytes bathed in a control medium was in the study of Rose and Schultz (69) shown to range from −15 to −55 mV, indicating considerable variance among cells.

Whereas our results indicate that use of parameter values from reported experimental data lead to a reasonable response in our model, it is not always possible to find a unanimous value for every parameter. Experimentalists do not always agree on one value, and the uncertainty can in some cases be significant. As an example, although several experiments have been done to estimate the turnover rate of SGLT1, there is little agreement on a consensus value (45). The rate in our model ($1–3\ s^{-1}$), which is based on parameters from Ref. 97, is in the lower region of reported values. A recent detailed modeling of the SGLT1 transport cycle (46) suggests that the rate should be higher ($35\ ^{-1}$). Similar discussion can be made for all the flow expressions used in this study. We have in general chosen to not include uncertain aspects in the rate expressions when good empirical data for various reasons have been lacking.

Regulatory Mechanisms and Na^+/K^+ Homeostasis

The presented model provides insight into how enterocytes maintain intracellular homeostasis even when confronted with changing rates of Na^+ inflow. It provides a useful framework for quantitative testing of plausible regulatory mechanisms in the enterocyte, in which the two controller motifs for Na-K-ATPase and K permeability presented here are examples of such.

When the inflow of Na^+ increases due to absorption of glucose, the enterocyte has to adapt the Na-K-ATPase-driven compensatory outflow of Na^+. Since the Na-K-ATPase also imports K^+ into the cell, an increase in Na-K-ATPase Na^+ outflow must be followed by an increase in K^+ outflow. If not, the enterocyte would be flooded by either Na^+ or K^+. The earlier mentioned experiments show that besides a transient

increase there is no sustained higher concentration of intracellular Na^+ ($[Na_c]$) during absorption of nutrients (30, 72). This means that the Na-K-ATPase-driven outflow has to increase by other means than mass action kinetics. The explanation suggested by our controller motif is that the transient increase in intracellular Na^+ brings about an increase in the number of active Na-K-ATPase proteins in the basolateral membrane. This can explain the results of Rokaw et al. (68), which show that the amount of Na-K-ATPase in A6 model cells for kidney collecting ducts epithelium is regulated in correspondence to inflow of Na^+.

The intracellular Na^+ activation of Na-K-ATPase synthesis has been shown for other cell types, where it increases the amount of mRNA coding for both the α- and β-subunits that combines into Na-K-ATPase (74, 98). Yamamoto et al. (98) showed that this increase, in cardiocytes, was directly caused by Na^+ due to Na^+-responsive sequences located within the 5′-flanking regions of the α-gene (α_1-, α_2-, and α_3-isoforms). Parallels can be drawn to the intestinal enterocytes as they express the α_1-isoform (44). Our simulations confirm that the regulation of Na-K-ATPase by intracellular Na^+ (Fig. 7) is a controller motif that is able to achieve homeostasis (10, 83), thus being a plausible mechanism for how the enterocytes manage to adapt and survive in a changing environment.

In addition to synthesis of Na-K-ATPase, posttranslational regulation by the insertion of preexisting transporter molecules from cytoplasmic storage pools can also be a contributing factor. Such regulation in response to intracellular Na^+ has been indicated in rabbit cortical collecting tubules (6). Given the many similarities between kidney and intestine epithelial cells, we cannot rule out the possibility that the abundance of membrane bound Na-K-ATPase in enterocytes is regulated by both translational and posttranslational pathways that are dependent on intracellular Na^+. Although we have focused on regulation by synthesis of new Na-K-ATPase in our argument, the ability of the controller to achieve homeostasis is coupled to the action where intracellular Na^+ regulates the number of active transporters and not to whether this happens by de novo synthesis or by insertion/activation of latent transporters.

Earlier work on sodium-transporting epithelial cells has speculated whether the relationship between the Na-K-ATPase turnover and intracellular Na^+ can be so steep that small changes in the latter may result in very large changes in the former (30, 72), enabling Na^+ outflow adaptation to occur without an increase in the amount of Na-K-ATPase. This alternative hypothesis is, however, considered unlikely and has also been shown to be incompatible with the experimental measurement of Na-K-ATPase kinetics (19, 54).

Nevertheless, an increase in the amount of Na-K-ATPase can possibly be induced by other means than direct activation by intracellular Na^+. Other mechanisms for the regulation of Na-K-ATPase are known; many studies have focused on the hormonal regulation through protein kinase A and C (PKA and PKC) pathways (see Ref. 80 for a review). Although important, hormonal mechanisms (involving sensing or prediction of the Na^+ inflow in enterocytes and secretion of hormones by some organ distant to the enterocyte) may be slower than the direct regulation by intracellular Na^+ and might thus play a secondary role. The effects of hormones on Na-K-ATPase activity have also been shown to be dependent on intracellular Na^+ in proximal tubule cells, suggesting that the level of intracellular Na^+ modulates whether hormones stimulate, inhibit, or have no effect on Na-K-ATPase levels (13).

A coupling between the activity of the Na-K-ATPase and the basolateral K permeability has been experimentally shown (7, 22). While this coupling has been confirmed for decades, it is still not clear what mechanism lies behind it (28). Our proposed regulatory motif (Fig. 8) is a minimal mechanism where ATP acts as a regulator. Since intracellular ATP concentration is dependent on the current ATP usage by Na-K-ATPase, i.e., the pump rate, the ATP concentration contains information about the inflow of K^+. ATP regulates the intracellular K^+ concentration by acting as an outflow controller modulating the outflow of K^+ through K_{ATP} channels, which are inhibited by ATP. This mechanism has only one intermediate between Na-K-ATPase pump rate and the basolateral K permeability.

Tsuchiya et al. (84) have reported that ATP is the main coupling modulator between Na-K-ATPase and K-channel activity in epithelial cells in the renal proximal tubule; they showed that an increase in Na-K-ATPase activity due to luminal addition of glucose and alanine leads to a 57% decrease in intracellular ATP, from 3.7 to 2.1 mM, followed by an increase in K conductance. Similar experiments (5) report of a reduction from 4.4 to 2.7 mM. These studies show that ATP-sensitive K_{ATP} channels react to a decrease in ATP caused by an increase in Na-K-ATPase activity during transcellular Na^+ transport. The role of ATP as a regulator is supported by the observation that an increase in K permeability is not seen in ATP-loaded proximal tubule cells (84). The kinetics of the inhibition by ATP has a K_I of 0.8 mM (in cardiac myocytes) (35). ATP-sensitive K channels have also been found in enterocytes (12). Our controller motif is based on the same type of coupling as is reported for ATP, and our results confirm that this is a mechanism that can provide homeostasis.

For simplicity we did only include consumption of ATP by the Na-K-ATPase. Other usage of ATP can, however, be included without changing the main results as long as these consumptions are approximately constant or increasing during nutrient transport. The only change is that the k_1^{ATP} parameter must be adjusted so that the synthesis and consumption balance each other at steady state.

The synthesis of ATP (see *Eq. 10*) must increase when the intracellular ATP concentration falls in order for the ATP concentration to reach a new steady state. If not, an increase in J^{NaK} will deplete the cell from ATP; the rate of consumption is in this case always greater than the rate of production. The increase in ATP synthesis with falling ATP concentration is conceivable as this will shift the ATP/ADP balance. The amount of ATP is reduced, and the amount of ADP available for new synthesis into ATP increases. A possible expansion of the current model would be the inclusion of differential equations describing the dynamic relations between ATP and ADP.

The reported (5, 84) and simulated (Fig. 10) reduction in intracellular ATP during transport may give reason to speculate whether it also directly affects the pump rate of Na-K-ATPase. Although possible, it is unlikely because studies in red blood cells, done by Marjonovic and Willis (53), have shown that the Na-K-ATPase is ATP saturated already at a concentration of 1.5 mM. The reduction in ATP during transport can thus regulate the K permeability and the outflow of K^+ without impeding the net transport by lowering the Na-K-ATPase pump rate. We have assumed that Na-K-ATPase is saturated

with respect to ATP in our model, i.e., the flow expression, *Eq. 2*, does not include [ATP].

Intracellular Ca^{2+} is another candidate for the regulation of K permeability; Ca^{2+} is known to increase the opening probability of enterocyte K channels (75), but no clear evidence has been given for a direct link between Na-K-ATPase activity and Ca^{2+}. Cell swelling has, however, been shown to increase the K permeability and interestingly this increase seems to be mediated by an increase in intracellular Ca^{2+} concentration together with a cell acidification (50). Cell swelling is not included in our enterocyte model, and we have therefore not examined this mechanism.

Other Regulatory Mechanisms

The regulation of cell volume is for enterocytes closely related to cell survivability during transport. The enterocyte has to react not only to an altered luminal nutrient load but also to a changing osmolarity. Exposing enterocytes to hypertonic additions of L-alanine and D-glucose elicits cell swelling followed by regulating volume decrease causing the cell to shrink to a smaller than initial size (50). Volume-activated Cl^- channels play an important part in this regulation, but volume regulation is not directly dependent on active transepithelial Na^+ transport or the operation of Na-K-ATPase (57). Many of the transporter proteins are also water transporters, e.g., SGLT1 (101) and GLUT2 (102). We kept the cell volume fixed in our model to make the modeling task feasible.

Being vital for cell survival, the regulation of intracellular ionic homeostasis must from the enterocyte's viewpoint have high priority. For the whole organism that the enterocyte is a part of, however, other transport-related regulatory mechanisms may have just as crucial implications. Regulation of the capacity of nutrient uptake, and the focus of nutrient uptake (sugar, proteins, or lipids), play major roles in securing organism survivability but are only of secondary importance for the enterocyte itself.

The capacity of the uptake system for glucose can be increased to respond to high luminal concentration. Studies have revealed intracellular stores of SGLT1 (38, 39), which are thought to play a role in the regulation of SGLT1-mediated glucose uptake. SGLT1 has also been shown to be rapidly upregulated by sweet taste receptors (76). In addition, there is evidence for trafficking of GLUT2 to the apical brush border membrane during high luminal glucose concentrations (48, 103). This makes GLUT2 a candidate responsible for the nonsaturable component of glucose uptake from the small intestine (36). Due to its properties as a facilitated transporter, GLUT2 can in contrast to SGLT1 only be used when the glucose concentration in the intestinal lumen is higher than inside the enterocyte. The usage of apical GLUT2 may be of advantage for the enterocyte; it enables the enterocyte to increase the glucose uptake without the ionic and osmotic challenges associated with the Na^+-coupled uptake through SGLT1.

Albeit not complete in describing the inner workings of every transporter protein, our model is able to combine the functions of each separate component. Understanding quantitatively not only how every component functions on its own but how their combined work mode integrates into a whole cell is an important part of physiology. Future work is needed to expand the model to include absorption and transport of other nutrients, such as fructose, amino acids, and fats, and the regulation of different uptake mechanisms and cell volume. This could provide insights into how the enterocyte handles combined absorption.

APPENDIX

Spatial Dimensions of an Absorbing Enterocyte

In its absorbing state the enterocytes have a form as shown in Fig. A1. The upper part is formed like a cylinder, and the lower part is formed like a truncated cone. The cross section of the cells are not perfectly rounded but shaped more like a polygonal giving the enterocytes a honeycomb shape that enables tighter packing than a circular shape (62). For calculations, however, it is adequate to assume a circular shape. For a rat enterocyte the typical dimensions are as in Ref. 62: r_m, radius at the mucosal top = 3.65 μm; r_s, radius at the serosal bottom = 1.9 μm; h_u, height of the tight junctions = 5 μm; and h_c, height of the cone = 28 μm. From these values we get an apical surface of 42 μm^2 (the effective absorptive area is roughly 20 times greater because of the microvilli), a basolateral surface area of the cone and the bottom of 500 μm^2, and a whole cell volume of roughly 900 μm^3. From the composition of enterocytes seen in electron micrographs (51), it is reasonable to assume that the cytoplasm occupies ~50% of the total cell volume (450 μm^3).

Estimation the Amount of SGLT1

To estimate the amount, or number, of SGLT1 transporters in enterocytes, we have used reported maximum absorption rates for active SGLT1-mediated uptake of glucose in jejunal sleeves, reviewed in Ref. 60. This rate varies between 8 to 23 $\mu mol \cdot h^{-1} \cdot cm^{-2}$ for small animals including mouse, rat, cat, and rabbit, where the smaller animals have higher absorption rates per surface area than larger animals. The absorption rates are given per centimeter squared of smooth mucosal area, which according to Pappenheimer (60) can be thought of as the area of an intestinal segment that has been distended to a circular cylinder. The effective surface area including the villi is three to eight times greater than the smooth surface area. For rats the absorption rate is between 12 to 20 $\mu mol \cdot h^{-1} \cdot cm^{-2}$ (60). Taking into account the increased surface due to the villi, using a factor of 5, and assuming that most of the villus area is covered with enterocytes, we estimate an absorption rate of 2.4 to 4 $\mu mol \cdot h^{-1} \cdot cm^{-2}$ of enterocyte covered surface area. A typical rat enterocyte has an apical radii of 3.65 μm (62), corresponding to a mucosal exposed surface of ~42 μm^2 (see *Spatial Dimensions of an Absorbing Enterocyte*).

From the above, and using a SGLT1 glucose transport rate of 1.5 s^{-1} ($9 \cdot 10^{-21}$ mol/h), we estimate that a single enterocyte contains around 100 to 250 million SGLT1 transporters. The estimate can be considered an average value over all enterocytes. We use 180 million SGLT1 transporters in our simulations.

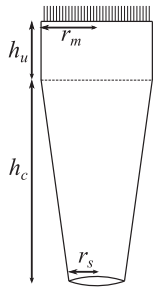

Fig. A1. The spatial dimensions of an enterocyte in absorbing state. The apical part of the cell has a cylindrical shape, and the lower part has is shaped like a truncated cone. See text for typical values of r_m, r_s, h_u, and h_c.

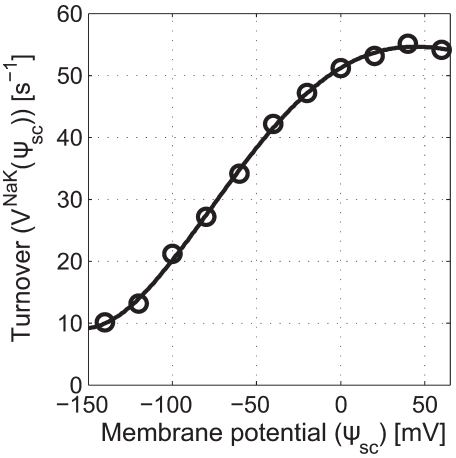

Fig. A2. Turnover rate for one single Na-K-ATPase protein as a function of serosal membrane potential, $V^{NaK}(\psi_{sc})$. The function is a 4th order polynomial fitted to the original data from the work of Gadsby and Nakao (19; reprinted with permisssion) (circles). The polynomial is $V^{NaK}(\psi_{sc}) = 5.46{\cdot}10^{-8}\psi_{sc}^4 - 2.43{\cdot}10^{-7}\psi_{sc}^3 - 2.00{\cdot}10^{-3}\psi_{sc}^2 + 0.16\psi_{sc} + 51$ (found by the Matlab function *polyfit*).

Voltage-Dependent Turnover of Na-K-ATPase

The polynomial for voltage-dependent turnover of Na-K-ATPase [$V^{NaK}(\psi_{sc})$] is plotted together with the experimental data from Gadsby and Nakao (19) in Fig. A2.

Adjustment of Kinetic Parameters for GLUT2

The kinetic parameters for GLUT2 reported by Maenz and Cheeseman (52) do not fit with the Haldane relationship, a point that remains uncommented on in their article. To ensure zero net flow at equal concentrations the Haldane relationship, $V_{max}^{G_c}K_{0.5}^{G_s} = V_{max}^{G_s}K_{0.5}^{G_c}$ must hold (8). Clearly the values from Maenz and Cheeseman cannot be used directly in our flow expression for GLUT 2 (*Eq. 4*) since this will lead to a rate expression for GLUT2 that makes it possible to have a passive transport of glucose against its concentration gradient. Still the kinetic data from Maenz and Cheeseman are to our knowledge the best available, because they are done on enterocyte GLUT2 from basolateral membrane vesicles, and consider both inflow and outflow. One possible explanation for the disagreement in the data from Maenz and Cheeseman is that the maximum outflow is underestimated; their article (52) states that the initial (maximum) rate of glucose outflow ($V_{max}^{G_c}$) was measured and averaged over a 10 s period, while the initial rate of glucose inflow ($V_{max}^{G_s}$) was measured and averaged over a shorter, 3-s period. Figure 2 from their original article (52) shows that the outflow sinks roughly 60% over 10 s, indicating that a 10-s average is an underestimate of the initial outflow. On this basis, we have chosen to use the half saturation constants ($K_{0.5}^{G_c}$) and ($K_{0.5}^{G_s}$) and the maximum inflow ($V_{max}^{G_s}$) directly as reported by Maenz and Cheeseman and adjusted the maximum glucose outflow ($V_{max}^{G_c}$) so that the Haldane relationship holds. In addition we have used the number for ^{3}H-cytochalasin B binding to the basolateral membrane (52), as an estimate of the number of GLUT2 transporters in the basolateral membrane vesicles that were studied by Maenz and Cheeseman. From this we can express the maximum inflow and outflow as molecules of glucose transporter per second for a single GLUT2 protein, and our calculations are shown below.

Maenz and Cheeseman (52) report the following values: maximum inflow ($V_{max}^{G_s}$): 1,138 pmol·mg protein^{-1}·s^{-1}; maximum outflow ($V_{max}^{G_c}$): 203 pmol·mg protein^{-1}·s^{-1}; half saturation constant for inflow ($K_{0.5}^{G_s}$): 48 mM; half saturation constant for outflow ($K_{0.5}^{G_c}$): 23 mM. We adjust the maximum outflow so that the Haldane relationship holds: Maximum outflow corrected for the Haldane relationship: 545 pmol·mg protein^{-1}·s^{-1}.

Maenz and Cheeseman further uses ^{3}H-cytochalasin B binding to the basolateral membrane as an estimate for the number of GLUT2 transporters. At saturated conditions the vesicles was found to bind 8.3 pmol/mg protein. Assuming a one-to-one relationship between the ^{3}H-cytochalasin B binding and the number of GLUT2 transporters we get the following: maximum inflow ($V_{max}^{G_s}$): 137 molecules of glucose per second ($8.19{\cdot}10^{-13}$ μmol/h); and maximum (corrected) outflow ($V_{max}^{G_c}$): 66 molecules of glucose per second ($3.95{\cdot}10^{-13}$ μmol/h) for one single GLUT2 transporter protein.

Iterative Calculation of Membrane Potentials

The iterative calculation of membrane potentials is based on the procedure outlined in Ref. 43. It utilizes two nested Newton-Raphson steps to refine the estimates until the conditions for cell and epithelial electroneutrality are met. The goal of the iterative calculation is to adjust the two independent membrane potentials so that both the cell current $I^c = \sum_i z_i(J_i^a + J_i^{bl})$ (*Eq. 7*) and the net epithelial current $I^e = \sum_i z_i(J_i^p - J_i^{bl})$ (*Eq. 8*) are sufficiently close to zero. The two loops are organized into an inner loop which adjusts ψ_{mc} so that $I^c(\psi_{mc}) = 0$, and an outer loop which adjusts ψ_{ms} so that $I^e(\psi_{ms}) = 0$.

The Newton-Raphson adjustments require the computation of the derivatives $dI^c(\psi_{mc})/d\psi_{mc}$ and $dI^e(\psi_{ms})/d\psi_{ms}$. We estimate these by calculating polynomial approximations of $I^c(\psi_{mc})$, treating ψ_{ms} and all the other parameters as constants, and $I^e(\psi_{ms})$, treating ψ_{mc} and all the other parameters as constants.

The procedure for the iterative method is as follows for each time step in the simulation:

1) Use the membrane potentials from the last time step as starting guesses.

2) Estimate ψ_{mc} and ψ_{ms} by two nested Newton-Raphson loops.

a) Find a polynomial approximation of the net cell current I^c as a function of ψ_{mc}. This is done by calculating the individual flows for a range of different ψ_{mc} values.

b) Estimate ψ_{mc} by an inner loop.

i) Calculate the individual flows for the current ψ_{mc} and ψ_{ms}.

ii) Calculate the apical and the basolateral membrane currents, $I^a = \sum_i z_i J_i^a$ and $I^{bl} = \sum_i z_i J_i^{bl}$.

iii) Calculate the net cell current $I^c = I^a + I^{bl}$.

iv) If $|I^c| = |\sum_i z_i(J_i^a + J_i^{bl})| < 10^{-9}$ pmol/h exit the inner loop with the current ψ_{mc} value. Otherwise update ψ_{mc} by a Newton-Raphson step: $\psi_{mc} = \psi_{mc} - I^c/[dI^c(\psi_{mc})/d\psi_{mc}]$ where the polynomial approximation of $I^c(\psi_{mc})$ is used to estimate the derivative and then restart the inner loop.

c) Find a polynomial approximation of the net epithelial current as a function of ψ_{ms}. This is done by calculating the individual flows for a range of different ψ_{ms} values.

d) Calculate the individual flows for the current ψ_{mc} and ψ_{ms}.

Table A1. *Flow expressions*

Protein	Flow expression
SGLT1	$J_{Na}^{SGLT} = -\frac{2n_{SGLT}}{1.672{\cdot}10^{14}}\left(\frac{\varepsilon[Na_m]^2[G_m]+\varphi[Na_m]^2+\gamma}{\alpha+\beta[G_m]+\chi[Na_m]^2+[Na_m]^2[G_m]}\right)$
Na-K-ATPase	$J^{Nak} = V^{NaK}(\psi_{sc}){\cdot}n_{NaK}{\cdot}\frac{1.13[Na_c]^{1.36}}{(K_{0.5}^{Na_c})^{1.36}+[Na_c]^{1.36}}{\cdot}\frac{1.3[K_s]}{K_{0.5}^{K_s}+[K_s]}$
Coupled NaCl	$J^{NaCl} = \frac{2V_{max}^{NaCl}([Na_m][Cl_m]-[Na_c][Cl_c])}{2K_1K_3+K_3[Na_m]+K_4[Cl_m]+2[Na_m][Cl_m]}$
GLUT2	$J^{GLUT} = \frac{V_{max}^{G_c}K_{0.5}^{G_s}[G_c]-V_{max}^{G_s}K_{0.5}^{G_c}[G_s]}{(K_{0.5}^{G_s}+[G_c])(K_{0.5}^{G_s}+[G_s])}{\cdot}n_{GLUT}$
Diffusive flows	$J_i^D = -\frac{P_i z_i F\psi}{RT}\left(\frac{[i_{out}]-[i_{in}]\exp(z_iF\psi/RT)}{1-\exp(z_iF\psi/RT)}\right){\cdot}A$

Table A2. *Parameters used in the simulations (if not stated otherwise)*

Cell size[a]	
V_c, cell (cytpoplasm volume)	450 μm^3
A^s, apical surface area	42 μm^2
A^a, apical absorptive membrane area	840 μm^2
A^{bl}, basolateral absorptive membrane area	500 μm^2
SGLT[b]	
Electrical coefficients	
α_1	0.3
α_2	0
δ	0.7
Rate constants	
k_{12}^0	140,000 $M^{-2} \cdot s^{-1}$
k_{23}	45,000 $M^{-1} \cdot s^{-1}$
k_{34}	50 s^{-1}
k_{45}	800 s^{-1}
k_{56}^0	5 s^{-1}
k_{61}^0	25 s^{-1}
k_{25}^0	0 s^{-1}
k_{21}^0	300 s^{-1}
k_{32}	20 s^{-1}
k_{43}	50 s^{-1}
k_{54}	77,778 $M^{-1} \cdot s^{-1}$
k_{65}^0	2,250 $M^{-2} \cdot s^{-1}$
k_{16}^0	600 s^{-1}
k_{52}^0	0 s^{-1}
The macro constants α, β, χ, ε, φ, and γ are given by *Eqs. A22–A28* in Ref. 65.	
Na-K-ATPase[c]	
V^{NaK}	Function of ψ_{sc}
$K_{0.5}^{Na_c}$	10 mM
$K_{0.5}^{K_s}$	1.5 mM
NaCl cotransport[d]	
V_{max}^{NaCl}	2.48 pmol/h
K_1	14 mM
K_3	22 mM
K_4	56 mM
GLUT2[e]	
$V_{max}^{G_c}$	$3.95 \cdot 10^{-13}$ μmol/h
$V_{max}^{G_s}$	$8.19 \cdot 10^{-13}$ μmol/h
$K_{0.5}^{G_c}$	23 mM
$K_{0.5}^{G_s}$	48 mM
Permeabilities[f]	
P_{Na}^a	$3.4 \cdot 10^{-4}$ cm/h
P_K^a	$3.0 \cdot 10^{-4}$ cm/h
P_{Cl}^a	$3.6 \cdot 10^{-4}$ cm/h
P_{Na}^p	$16 \cdot 10^{-2}$ cm/h
P_K^p	$18 \cdot 10^{-2}$ cm/h
P_{Cl}^p	$9.0 \cdot 10^{-2}$ cm/h
P_{Na}^{bl}	$3.6 \cdot 10^{-4}$ cm/h
P_K^{bl}	$14.6 \cdot 10^{-3}$ cm/h
P_{bl}^{Cl}	$2.6 \cdot 10^{-3}$ cm/h
Mucosal and serosal concentrations[g]	
$[G_m]$	0.1–20 mM
$[K_m]$	5.4 mM
$[G_s]$	10 mM
$[K_s]$	5.4 mM
$[Na_m]$	140 mM
$[Cl_m]$	103 mM
$[Na_s]$	140 mM
$[Cl_s]$	103 mM
Cell variables	
Initial concentrations[h]	
$[G_c]$	12 mM
$[K_c]$	129 mM
$[ATP_c]$	4 mM
$[Na_c]$	49 mM
$[Cl_c]$	57 mM
Amount of protein[i]	
n_{SGLT}	$180 \cdot 10^6$
n_{GLUT}	$13.2 \cdot 10^6$
n_{NaK}	$49.2 \cdot 10^5$
Regulatory parameters[j]	
Regulation of Na-K-ATPase	
k_{NaK}	$5.6 \cdot 10^5$ $mM^{-1} \cdot h^{-1}$
$K_{0.5}^{EsetNaK}$	10^4
$V_{max}^{EsetNaK}$	$2.74 \cdot 10^7$ h^{-1}
Regulation of basolateral K-permeability	
k_1^{ATP}	10.2 pmol/h
K_1^{ATP}	0.8 mM
$K_{0.5}{}^{ATP}$	0.5 mM
P_{Kmax}^{bl}	$87.6 \cdot 10^{-3}$ cm/h
Other parameters	
F	96,485 C/mol
T	310.15 K
R	8.314 $JK^{-1} \cdot mol^{-1}$

Table footnote: [a]See *Spatial Dimensions of an Absorbing Enterocyte.* [b]Parameters are taken from Ref. 97. However, we had to adjust the k_{54} value to keep microscopic reversibility. The macro constants α, β, χ, ε, φ, and γ are functions of the rate constants, the concentration of intracellular Na^+ ($[Na_c]$), intracellular glucose ($[G_c]$), and the membrane potential (ψ_{mc}). They thus change during simulation, but typical values are α, $1.2 \cdot 10^{-6}$; β, $0.8 \cdot 10^{-6}$; χ, $2 \cdot 10^{-4}$; ε, -0.94; φ, 0; γ, $2.2 \cdot 10^{-6}$ (at end of the long-term simulation). [c]V^{NaK}, see Ref. 19 and *Voltage-Dependent Turnover of Na-K-ATPase.* $K_{0.5}$, see Ref. 54. [d]See Ref. 55, V_{max}^{NaCl} is adjusted so that the coupled NaCl transport makes up ~30% of the total Na^+ inflow during glucose absorption ($[G_m] = 10$ mM). [e]See Ref. 52 and *Adjustment of Kinetic Parameters for GLUT2.* [f]*Integrative Model.* [g]See Refs. 19 and 23. The serosal glucose concentration $[G_s]$ is assumed to be 10 mM under light glucose load; the value is around twice that of arterial blood in a near fastening state. (According to Ref. 61 the concentration of glucose in villus capillary can reach up to 30 mM under heavy glucose load.) [h]Initial concentrations used in all simulation except the simulation of short-term change in mucosal sodium where the following was used $[G_c] = 15$ mM, $[Na_c] = 63$ mM, $[K_c] = 116$ mM, and $[Cl_c] = 60$ mM. The initial concentrations are selected close to the steady-state concentrations to avoid startup transients. The figures in RESULTS do not show the startup transients. [i]See *Estimation the Amount of SGLT1* for n_{SGLT}; the other amounts are estimates based on numbers needed to respond to the inflow of glucose and sodium. The amount of Na-K-ATPase is in the range reported for rabbit kidney cells (34). [j]These parameters are selected to achieve reasonable setpoints and dynamic response (10).

e) Calculate the current over the basolateral membrane, $I^{bl} = \sum_i z_i J_i^{bl}$, and the paracellular current, $I^p = \sum_i z_i J_i^p$.

f) Calculate the net epithelial current $I^e = I^p - I^{bl}$.

g) If $|I^e| = |\sum_i z_i (J_i^p + J_i^{bl})| < 10^{-9}$ pmol/h exit the outer loop with the current ψ_{ms}. Otherwise update ψ_{ms} by a Newton-Raphson step: $\psi_{ms} = \psi_{ms} - I^e/[dI^e(\psi_{ms})/d\psi_{ms}]$, where the polynomial approximation of $I^e(\psi_{ms})$ is used to estimate the derivative and then restart the outer loop.

3) The conditions for electroneutrality are now met. Calculate $\psi_{sc} = \psi_{mc} - \psi_{ms}$. Output the flows so that they can be integrated to the next time step.

The Newton-Raphson seek is stopped once the net cell current and the net epithelial current are sufficiently close to zero. We have used the following criteria:

$$\left|I^c\right| = \left|\sum_i z_i \left(J_i^a + J_i^{bl}\right)\right| < 10^{-9}\text{pmol/h}$$
$$\left|I^e\right| = \left|\sum_i z_i \left(J_i^p - J_i^{bl}\right)\right| < 10^{-9}\text{pmol/h} \qquad (A1)$$

For our enterocyte, which has a volume of 450 μm^3, these criteria correspond to a maximum charge difference of 2.22 nM/h (monovalent ions). A charge unbalance in this order will only affect the membrane potential by a few tens of a microvolt.

The iterative procedure was tested and verified by simulating the enterocyte model under conditions where the membrane potential can

be analytically calculated by the Goldman-Hodkin-Katz equation for membrane potential (70). The paracellular permeability was set to zero, and only diffusion of Na^+, K^+, and Cl^- was considered, i.e., no active transport or cotransport. Simulation of these conditions produced the exact same membrane potentials as the analytical solution (results not shown).

The nested procedure can be time consuming since ψ_{mc} has to be fully optimized for each new and improved estimate of ψ_{ms}. Nevertheless, in practice the Newton-Raphson method quickly converges and needs mostly less than a total of 10 iterations of the inner loop in our simulations.

Model Equations

The following differential equations describes the dynamical states

$$\left[\dot{G}_c\right] = \frac{1}{V_c}\left(\frac{1}{2}J_{Na}^{SGLT} - J^{GLUT}\right) \quad (A2)$$

$$\left[\dot{Na}_c\right] = \frac{1}{V_c}\left(J_{Na}^{SGLT} - 3J^{NaK} + J^{NaCl} + J_{Na}^{Da} + J_{Na}^{Dbl}\right) \quad (A3)$$

$$\left[\dot{K}_c\right] = \frac{1}{V_c}\left(2J^{NaK} + J_{K}^{Da} + J_{K}^{Dbl}\right) \quad (A4)$$

$$\left[\dot{Cl}_c\right] = \frac{1}{V_c}\left(J^{NaCl} + J_{Cl}^{Da} + J_{Cl}^{Dbl}\right) \quad (A5)$$

where the different flow expressions (J) are given in Table A1, and the parameters are given in Table A2. The model is expanded by *Eqs. 9* to *11* in the main text to account for regulation of intracellular Na^+ and K^+.

ACKNOWLEDGMENTS

We thank Ingunn W. Jolma for advice and comments. We also thank the anonymous reviewers for meticulous examination of the work and for helpful comments.

DISCLOSURES

No conflicts of interest, financial or otherwise, are declared by the author(s).

AUTHOR CONTRIBUTIONS

Author contributions: K.T. conception and design of research; K.T. and T.D. performed experiments; K.T., T.D., and P.R. analyzed data; K.T. and P.R. interpreted results of experiments; K.T. prepared figures; K.T. drafted manuscript; K.T., T.D., and P.R. edited and revised manuscript; K.T., T.D., and P.R. approved final version of manuscript.

REFERENCES

1. **Baerentsen H, Giraldez F, Zeuthen T.** Influx mechanisms for Na^+ and Cl^- across the brush border membrane of leaky epithelia: A model and microelectrode study. *J Membr Biol* 75: 205–218, 1983.
2. **Baerentsen HJ, Christensen O, Thomsen GP, Zeuthen T.** Steady States and the effects of ouabain in the necturus gallbladder epithelium: a model analysis. *J Membr Biol* 225: 215–225, 1982.
3. **Baker GF, Widdas WF.** The asymmetry of the facilitated transfer system for hexoses in human red cells and the simple kinetics of a two component model. *J Physiol* 231: 143–165, 1973.
4. **Barry RJ, Eggenton J.** Ionic basis of membrane potentials of epithelial cells in rat small intestine. *J Physiol* 227: 217–231, 1972.
5. **Beck JS, Breton S, Mairbaurl H, Laprade R, Giebisch G.** Relationship between sodium transport and intracellular ATP in isolated perfused rabbit proximal convoluted tubule. *Am J Physiol Renal Fluid Electrolyte Physiol* 261: F634–F639, 1991.
6. **Blot-Chabaud M, Wanstok F, Bonvalet JP, Farman N.** Cell sodium-induced recruitment of Na^+-K^+-ATPase pumps in rabbit cortical collecting tubules is aldosterone-dependent. *J Biol Chem* 265: 11676–11681, 1990.
7. **Brown PD, Sepúlveda FV.** Potassium movements associated with amino acid and sugar transport in enterocytes isolated from rabbit jejunum. *J Physiol* 363: 271–285, 1985.
8. **Cornish-Bowden A.** *Fundamentals of Enzyme Kinetics* (2nd ed) London, UK: Portland, 1995.
9. **Davis PK, Wu G.** Compartmentation and kinetics of urea cycle enzymes in porcine enterocytes. *Comp Biochem Physiol B Biochem Mol Biol* 119: 527–537, 1998.
10. **Drengstig T, Jolma IW, Ni XY, Thorsen K, Xu XM, Ruoff P.** A basic set of homeostatic controller motifs. *Biophys J* 103: 2000–2010, 2012.
11. **Drengstig T, Ueda RH, Ruoff P.** Predicting perfect adaptation motifs in reaction kinetic networks. *J Phys Chem B* 112: 16752–16758, 2008.
12. **Dubinsky WP, Mayorga-wark O, Schultz SG, Heitzmann D, Warth R.** Potassium channels in basolateral membrane vesicles from Necturus enterocytes: stretch and ATP sensitivity. *Am J Physiol Cell Physiol* 279: C634–C638, 2000.
13. **Efendiev R, Bertorello AM, Zandomeni R, Cinelli AR, Pedemonte CH.** Agonist dependent regulation of renal Na^+,K^+-ATPase activity is modulated by intracellular sodium concentration. *J Biol Chem* 277: 11489–11496, 2002.
14. **Eskandari S, Wright EM, Loo DD.** Kinetics of the reverse mode of the Na^+/glucose cotransporter. *J Membr Biol* 204: 23–32, 2005.
15. **Fan CC, Faust RG, Powell DW.** Coupled sodium-chloride transport by rabbit ileal brush border membrane vesicles. *Am J Physiol Gastrointest Liver Physiol* 244: G375–G385, 1983.
16. **Frizzell RA, Field M, Schultz SG.** Sodium-coupled chloride transport by epithelial tissues. *Am J Physiol Renal Fluid Electrolyte Physiol* 236: F1–F8, 1979.
17. **Frizzell RA, Schultz SG.** Ionic conductances of extracellular shunt pathway in rabbit ileum. Influence of shunt on transmural sodium transport and electrical potential differences. *J Gen Physiol* 59: 318–346, 1972.
18. **Frizzell RA, Smith PL, Vosburgh E, Field M.** Coupled sodium-chloride influx across brush border of flounder intestine. *J Membr Biol* 46: 27–39, 1979.
19. **Gadsby DC, Nakao M.** Steady-state current-voltage relationship of the Na/K pump in guinea pig ventricular myocytes. *J Gen Physiol* 94: 511–537, 1989.
20. **Glynn IM.** A hundred years of sodium pumping. *Annu Rev Physiol* 64: 1–18, 2002.
21. **Goldner AM, Schultz SG, Curran PF.** Sodium and sugar fluxes across the mucosal border of rabbit ileum. *J Gen Physiol* 53: 362–383, 1969.
22. **Grasset E, Gunter-Smith P, Schultz SG.** Effects of Na-coupled alanine transport on intracellular K activities and the K conductance of the basolateral membranes of Necturus small intestine. *J Membr Biol* 94: 89–94, 1983.
23. **Guyton AC, Hall JE.** *Textbook of Medical Physiology* (11th ed). Philadelphia, PA: Elsevier Saunders, 2006.
24. **Hammerton RW, Krzeminski KA, Mays RW, Ryan TA, Wollner DA, Nelson WJ.** Mechanism for regulating cell surface distribution of Na^+,K^+-ATPase in polarized epithelial cells. *Science* 254: 847–850, 1991.
25. **Hartmann T, Verkman AS.** Model of ion transport regulation in chloride-secreting airway epithelial cells. Integrated description of electrical, chemical, and fluorescence measurements. *Biophys J* 58: 391–401, 1990.
26. **Hayashi H, Suruga K, Yamashita Y.** Regulation of intestinal Cl^-/HCO_3^- exchanger SLC26A3 by intracellular pH. *Am J Physiol Cell Physiol* 296: C1279–C1290, 2009.
27. **Hayashi H, Szászi K, Grinstein S.** Multiple modes of regulation of Na^+/H^+ exchangers. *Ann NY Acad Sci* 976: 248–258, 2002.
28. **Heitzmann D, Warth R.** Physiology and pathophysiology of potassium channels in gastrointestinal epithelia. *Physiol Rev* 88: 1119–1182, 2008.
29. **Hirayama BA, Lostao MP, Panayotova-Heiermann M, Loo DD, Turk E, Wright EM.** Kinetic and specificity differences between rat, human, and rabbit Na^+-glucose cotransporters (SGLT-1). *Am J Physiol Gastrointest Liver Physiol* 270: G919–G926, 1996.
30. **Hudson RL, Schultz SG.** Sodium-coupled sugar transport: effects on intracellular sodium activities and sodium-pump activity. *Science* 224: 1237–1239, 1984.
31. **Ikeda TS, Hwang ES, Coady MJ, Hirayama BA, Hediger MA, Wright EM.** Characterization of a Na^+/glucose cotransporter cloned from rabbit small intestine. *J Membr Biol* 110: 87–95, 1989.

32. **Ilundain A, Lluch M, Ponz F.** Kinetics of intestinal sugar transport, in vivo. *Rev Esp Fisiol* 35: 359–366, 1979.
33. **Isenberg JI, Ljungstrom M, Safsten B, Flemstrom G.** Proximal duodenal enterocyte transport: evidence for Na^+-H^+ and Cl^--HCO_3^- exchange and $NaHCO_3$ cotransport. *Am J Physiol Gastrointest Liver Physiol* 264: G677–G685, 1993.
34. **Jørgensen PL.** Structure, function and regulation of Na,K-ATPase in the kidney. *Kidney Int* 29: 10–20, 1986.
35. **Kabakov AY.** Activation of K_{ATP} channels by Na/K pump in isolated cardiac myocytes and giant membrane patches. *Biophys J* 75: 2858–2867, 1998.
36. **Kellett GL.** The facilitated component of intestinal glucose absorption. *J Physiol* 531: 585–595, 2001.
37. **Kessler M, Semenza G.** The small-intestinal Na^+,D-glucose cotransporter: an asymmetric gated channel (or pore) responsive to $\Delta\Psi$. *J Membr Biol* 76: 27–56, 1983.
38. **Khoursandi S, Scharlau D, Herter P, Kuhnen C, Martin D, Kinne RK, Kipp H.** Different modes of sodium-D-glucose cotransporter-mediated D-glucose uptake regulation in Caco-2 cells. *Am J Physiol Cell Physiol* 287: C1041–C1047, 2004.
39. **Kipp H, Khoursandi S, Scharlau D, Kinne RK.** More than apical: distribution of SGLT1 in Caco-2 cells. *Am J Physiol Cell Physiol* 285: C737–C749, 2003.
40. **Knickelbein R, Aronson PS, Atherton W, Dobbins JW.** Sodium and chloride transport across rabbit ileal brush border. I. Evidence for Na-H exchange. *Am J Physiol Gastrointest Liver Physiol* 245: G504–G510, 1983.
41. **Knickelbein R, Aronson PS, Schron CM, Seifter J, Dobbins JW.** Sodium and chloride transport across rabbit ileal brush border. II. Evidence for Cl-HCO_3 exchange and mechanism of coupling. *Am J Physiol Gastrointest Liver Physiol* 249: G236–G245, 1985.
42. **Knudsen OS.** *Biological Membranes Theory of Transport, Potentials and Electric Impulses*. Cambridge, UK: Cambridge Univ Press, 2007.
43. **Latta R, Clausen C, Moore LC.** General method for the derivation and numerical solution of epithelial transport models. *J Membr Biol* 82: 67–82, 1984.
44. **Lingrel JB.** Na,KATPase: isoform structure, function, expression. *J Bioenerg Biomembr* 24: 263–270, 1992.
45. **Longpré JP, Lapointe JY.** Determination of the Na^+/glucose cotransporter (SGLT1) turnover rate using the ion-trap technique. *Biophys J* 100: 52–59, 2011.
46. **Longpré JP, Sasseville LJ, Lapointe JY.** Simulated annealing reveals the kinetic activity of SGLT1, a member of the LeuT structural family. *J Gen Physiol* 140: 361–374, 2012.
47. **Loo DD, Hirayama BA, Cha A, Bezanilla F, Wright EM.** Perturbation analysis of the voltage-sensitive conformational changes of the Na^+/glucose cotransporter. *J Gen Physiol* 125: 13–36, 2005.
48. **Mace OJ, Affleck J, Patel N, Kellett GL.** Sweet taste receptors in rat small intestine stimulate glucose absorption through apical GLUT2. *J Physiol* 582: 379–392, 2007.
49. **Macey RI, Moura TF.** Basic principles of transport. In: *Handbook of Physiology. Cell Physiology*, edited by Hoffman J, Jamieson J. Bethesda, MD: Am Physiol Soc, 1997, sect 14, chapt 6.
50. **MacLeod RJ, Hamilton JR.** Volume regulation initiated by Na^+-nutrient cotransport in isolated mammalian villus enterocytes. *Am J Physiol Gastrointest Liver Physiol* 260: G26–G33, 1991.
51. **Madara JL, Pappenheimer JR.** Structural basis for physiological regulation of paracellular pathways in intestinal epithelia. *J Membr Biol* 100: 149–164, 1987.
52. **Maenz DD, Cheeseman CI.** The Na^+-independent D-glucose transporter in the enterocyte basolateral membrane: orientation and cytochalasin B binding characteristics. *J Membr Biol* 97: 259–266, 1987.
53. **Marjanovic M, Willis JS.** Is the pump of intact red blood cells saturated for ATP at physiological concentrations? In: *The Sodium Pump: Recent Developments–Society of General Physiologists 44th Annual Symposium*, edited by Kaplan JH, Weer PD. New York, NY: Rockefeller Univ Press, 1990, p. 457–459.
54. **Nakao M, Gadsby DC.** [Na] and [K] dependence of the Na/K pump current-voltage relationship in guinea pig ventricular myocytes. *J Gen Physiol* 94: 539–565, 1989.
55. **Nellans HN, Frizzell RA, Schultz SG.** Coupled sodium-chloride influx across the brush border of rabbit ileum. *Am J Physiol* 225: 467–475, 1973.
56. **Nellans HN, Frizzell RA, Schultz SG.** Brush-border processes and transepithelial Na and Cl transport by rabbit ileum. *Am J Physiol* 226: 1131–1141, 1974.
57. **Nellans HN, Schultz SG.** Relations 1189 among transepithelial sodium transport, potassium exchange, and cell volume in rabbit ileum. *J Gen Physiol* 68: 441–463, 1976.
58. **Ni XY, Drengstig T, Ruoff P.** The control of the controller: molecular mechanisms for robust perfect adaptation and temperature compensation. *Biophys J* 97: 1244–1253, 2009.
59. **Okada Y, Sato T, Inouye A.** Effects of potassium ions and sodium ions on membrane potential of epithelial cells in rat duodenum. *Biochim Biophys Acta* 413: 104–115, 1975.
60. **Pappenheimer JR.** Scaling of dimensions of small intestines in non-ruminant eutherian mammals and its significance for absorptive mechanisms. *Comp Biochem Physiol A Mol Integr Physiol* 121: 45–58, 1998.
61. **Pappenheimer JR.** Intestinal absorption of hexoses and amino acids: from apical cytosol to villus capillaries. *J Membr Biol* 184: 233–239, 2001.
62. **Pappenheimer JR, Michel CC.** Role of villus microcirculation in intestinal absorption of glucose: coupling of epithelial with endothelial transport. *J Physiol* 553: 561–574, 2003.
63. **Pappenheimer JR, Reiss KZ.** Contribution of solvent drag through intercellular junctions to absorption of nutrients by the small intestine of the rat. *J Membr Biol* 100: 123–136, 1987.
64. **Parent L, Supplisson S, Loo DD, Wright EM.** Electrogenic properties of the cloned Na^+/glucose cotransporter: I. Voltage-clamp studies. *J Membr Biol* 62: 49–62, 1992.
65. **Parent L, Supplisson S, Loo DD, Wright EM.** Electrogenic properties of the cloned Na^+/glucose cotransporter: II. A transport model under nonrapid equilibrium conditions. *J Membr Biol* 125: 63–79, 1992.
66. **Rakowski RF, Gadsby DC, De Weer P.** Stoichiometry and voltage dependence of the sodium pump in voltage-clamped, internally dialyzed squid giant axon. *J Gen Physiol* 93: 903–941, 1989.
67. **Reuss L.** Epithelial transport. In: *Handbook of Physiology. Cell Physiology*, edited by Hoffman JF, Jamieson JD. Bethesda, MD: Am Physiol Soc, 1997, sect 14, chapt 8, p. 308–388.
68. **Rokaw MD, Sarac E, Lechman E, West M, Angeski J, Johnson JP, Zeidel ML.** Chronic regulation of transepithelial Na^+ transport by the rate of apical Na^+ entry. *Am J Physiol Cell Physiol* 270: C600–C607, 1996.
69. **Rose RC, Schultz SG.** Studies on the electrical potential profile across rabbit ileum effects of sugars and amino acids on transmural and transmucosal electrical potential difference. *J Gen Physiol* 57: 639–663, 1971.
70. **Schultz SG.** *Basic Principles of Membrane Transport*. Cambridge, UK: Cambridge Univ Press, 1980.
71. **Schultz SG.** Cellular models of epithelial ion transport. In: *Membrane Transport Processes in Organized Systems*, edited by Andreoli TE, Hoffman JF, Fanestil DD, Schultz SG. New York, NY: Plenum, 1987, p. 135–150.
72. **Schultz SG, Hudson RL.** How do sodium-absorbing cells do their job and survive? *Physiology* 1: 185–189, 1986.
73. **Schultz SG, Hudson RL.** Biology of sodium-absorbing epithelial cells: dawning of a new era. In: *Handbook of Physiology. The Gastrointestinal System. Intestinal Absorption and Secretion*. Bethesda, MD: Am. Physiol. Soc, 1991, sect 6, vol IV, chap 2, p. 45–81.
74. **Senatorov VV, Stys PK, Hu B.** Regulation of Na^+,K^+-ATPase by persistent sodium accumulation in adult rat thalamic neurones. *J Physiol* 525: 343–353, 2000.
75. **Sepúlveda FV, Mason WT.** Single channel recordings obtained from basolateral membranes of isolated rabbit enterocytes. *FEBS Lett* 191: 87–91, 1985.
76. **Stearns AT, Balakrishnan A, Rhoads DB, Tavakkolizadeh A.** Rapid upregulation of sodium-glucose transporter SGLT1 in response to intestinal sweet taste stimulation. *Ann Surg* 251: 865–871, 2010.
77. **Stein WD.** *Transport and Diffusion Across Cell Membranes*. Orlando, FL: Academic, 1986.
78. **Stephenson JL, Tewarson RP, Mejia R.** Quantitative analysis of mass and energy balance in non-ideal models of the renal counterflow system. *Proc Natl Acad Sci USA* 71: 1618–1622, 1974.
79. **Striling CE.** Radioautographic localization of sodium pump sites in rabbit intestine. *J Cell Biol* 53: 704–714, 1972.
80. **Therien AG, Blostein R.** Mechanisms of sodium pump regulation. *Am J Physiol Cell Physiol* 279: C541–C566, 2000.

81. **Thorens B, Cheng ZQ, Brown D, Lodish HF.** Liver glucose transporter: a basolateral protein in hepatocytes and intestine and kidney cells. *Am J Physiol Cell Physiol* 259: C279–C285, 1990.
82. **Thorens B, Mueckler M.** Glucose transporters in the 21st Century. *Am J Physiol Endocrinol Metab* 298: E141–E145, 2010.
83. **Thorsen K, Ruoff P, Drengstig T.** Control theoretic properties of physiological controller motifs. In: *Proceedings of the 2013 International Conference on System Science and Engineering (ICSSE)*, 2013, p. 165–170, doi:10.1109/ICSSE.2013.6614653.
84. **Tsuchiya K, Wang W, Giebisch G, Welling PA.** ATP is a coupling modulator of parallel Na,K-ATPase-K-channel activity in the renal proximal tubule. *Proc Natl Acad Sci USA* 89: 6418–6422, 1992.
85. **Verkman AS, Alpern RJ.** Kinetic transport model for cellular regulation of pH and solute concentration in the renal proximal tubule. *Biophys J* 51: 533–546, 1987.
86. **Warth R, Barhanin J.** Function of K^+ channels in the intestinal epithelium. *J Membr Biol* 193: 67–78, 2003.
87. **Weinstein AM.** Nonequilibrium thermodynamic model of the rat proximal tubule epithelium. *Biophys J* 44: 153–170, 1983.
88. **Weinstein AM.** Glucose transport in a model of the rat proximal tubule epithelium. *Math Biosci* 76: 87–115. 1985.
89. **Weinstein AM.** A mathematical model of the rat proximal tubule. *Am J Physiol Renal Fluid Electrolyte Physiol* 250: F860–F873, 1986.
90. **Weinstein AM.** Chloride transport in a mathematical model of the rat proximal tubule. *Am J Physiol Renal Fluid Electrolyte Physiol* 263: F784–F798, 1992.
91. **Weinstein AM.** Ammonia transport in a mathematical model of rat proximal tubule. *Am J Physiol Renal Physiol* 267: F237–F248, 1994.
92. **Weinstein AM.** A kinetically defined Na^+/H^+ antiporter within a mathematical model of the rat proximal tubule. *J Gen Physiol* 105: 617–641, 1995.
93. **Weinstein AM.** Modeling epithelial cell homeostasis: steady-state analysis. *Bull Math Biol* 61: 1065–1091, 1999.
94. **Weinstein AM.** A mathematical model of the outer medullary collecting duct of the rat. *Am J Physiol Renal Physiol* 279: F24–F45, 2000.
95. **Weinstein AM.** Modeling epithelial cell homeostasis: assessing recovery and control mechanisms. *Bull Math Biol* 66: 1201–1240, 2004.
96. **Weinstein AM, Stephenson JL.** Electrolyte transport across a simple epithelium. Steady state and transient analysis. *Biophys J* 27: 165–186, 1979.
97. **Wright EM, Loo DD, Hirayama BA.** Biology of human sodium glucose transporters. *Physiol Rev* 91: 733–794, 2011.
98. **Yamamoto K, Ikeda U, Seino Y, Tsuruya Y, Oguchi A, Okada K, Ishikawa S, Saito T, Kawakami K, Hara Y, Shimada K.** Regulation of Na,K-adenosine triphosphatase gene expression by sodium ions in cultured neonatal rat cardiocytes. *J Clin Invest* 92: 1889–1895, 1993.
99. **Yoshikawa T, Inoue R, Matsumoto M, Yajima T, Ushida K, Iwanaga T.** Comparative expression of hexose transporters (SGLT1, GLUT1, GLUT2 and GLUT5) throughout the mouse gastrointestinal tract. *Histochem Cell Biol* 135: 183–194, 2011.
100. **Zachos NC, Tse M, Donowitz M.** Molecular physiology of intestinal Na^+/H^+ exchange. *Annu Rev Physiol* 67: 411–443, 2005.
101. **Zeuthen T, Meinild AK, Loo DD, Wright EM, Klaerke DA.** Isotonic transport by the Na^+-glucose cotransporter SGLT1 from humans and rabbit. *J Physiol* 531: 631–644, 2001.
102. **Zeuthen T, Zeuthen E, Macaulay N.** Water transport by GLUT2 expressed in Xenopus laevis oocytes. *J Physiol* 579: 345–361, 2007.
103. **Zheng Y, Scow JS, Duenes JA, Sarr MG.** Mechanisms of glucose uptake in intestinal cell lines: role of GLUT2. *Surgery* 151: 13–25, 2012.